Radiative Darcy-Forchheimer squeezing carbon nanotubes suspended nanofluid flow between parallel disks

Thesis Submitted By

NOMANA ABID
(01-248181-004)

Supervised By

Prof. Dr. M. Ramzan

A dissertation submitted to the Department of Computer Science, Bahria University, Islamabad as a partial fulfillment of the requirements for the award of the degree of MS (Mathematics)

Session (2018-2020)

Bahria University
Discovering Knowledge

MS-13

Thesis Completion Certificate

Student's Name: **Nomana Abid** Registration No: **56134** Programme of Study: **MS Mathematics**

Thesis Title: **Radiative Darcy-Forchheimer squeezing carbon nanotubes suspended nanofluid flow between parallel disks.**

It is to certify that the above student's thesis has been completed to my satisfaction and, to my belief, its standard is appropriate for submission for Evaluation. I have also conducted plagiarism test of this thesis using HEC prescribed software and found similarity index at **12%** that is within the permissible limit set by the HEC for the MS/MPhil degree thesis. I have also found the thesis in a format recognized by the BU for the MS/MPhil thesis.

Principal Supervisor's Signature: _____

Date: 4-2-2020 Name: Prof. Dr. M. Ramazan

Bahria University
Discovering Knowledge

MS-14A

Author's Declaration

I, **Nomana Abid** hereby state that my PhD thesis titled "**Radiative Darcy-Forchheimer squeezing carbon nanotubes suspended nanofluid flow between parallel disks**" is my own work and has not been submitted previously by me for taking any degree from this university **Bahria University** or anywhere else in the country/world.

At any time if my statement is found to be incorrect even after my Graduate the university has the right to withdraw/cancel my PhD degree.

Name of student: **Nomana Abid**

Date: **4-2-2020**

Bahria University
Discovering Knowledge

MS-14B

Plagiarism Undertaking

I, solemnly declare that research work presented in the thesis titled "**Radiative Darcy-Forchheimer squeezing carbon nanotubes suspended nanofluid flow between parallel disks**" is solely my research work with no significant contribution from any other person. Small contribution/help wherever taken has been duly acknowledged and that complete thesis has been written by me.

I understand the zero tolerance policy of the HEC and Bahria University towards plagiarism. Therefore, I as an Author of the above titled thesis declare that no portion of my thesis has been plagiarized and any material used as reference is properly referred/cited.

I undertake that if I am found guilty of any formal plagiarism in the above titled thesis even after award of PhD degree, the university reserves the right to withdraw/revoke my PhD degree and that HEC and the University has the right to publish my name on the HEC/University website on which names of students are placed who submitted plagiarized thesis.

Student/Author's Sign:

Name of the Student: **Nomana Abid**

Dedicated to

My Beloved Parents

and

Respected Supervisor

Acknowledgments

Everlasting praise to **ALLAH** the most Gracious, the most merciful who bestowed me with His great blessings. He who says in the Quran,

“Indeed, I am near. I respond to the invocation of the supplicant when someone calls upon me.’’ (Surah AL-Baqarah; Ayat:186)

I am really Blessed as He gave me the ability to think even upon a tiny thing He created. He gave me a source (His beloved **Prophet (PBUH)**) of light for my way to Him.

My acknowledgment is to my kind and a little bit strict supervisor, Prof. Dr. M. Ramzan, who supported me with his great opinions and inspirational thoughts. My intense gratitude is to my great teachers. In particular, Dr. Jafar Hasnain who encouraged me and helped me to see what I could be and Dr. Rizwan-ul-haq who prayed for me to become a good researcher. I’m blessed to have them in my life...

I would like to express my special thanks to my seniors Phd students who were always remained helpful to me and my fellows Nosheen and specially Ani Abida as she was always like a mother to me. May Allah shower His blessings upon them more than enough.

Nomana Abid

Bahria University Islamabad, Pakistan

February 4, 2020

Abstract

This study aims to investigate the time dependent squeezing flow of nano-fluid flow comprising carbon-nanotubes (CNTs) of dual nature say single-walled carbon-nanotubes (SWCNTs) and multi-walled carbon-nanotubes (MWCNTs) amidst two parallel disks. The upper disk is moving (towards and away) from the lower stationary and permeable disk. Numerical simulations of the proposed model are conducted accompanied by Cattaneo-Christov (CC) heat flux in a Darcy-Forchheimer permeable media. Additional impacts of homogeneous-heterogeneous (HH) reactions are also taken with melting heat. Relevant transformations procedure is implemented for the transition of partial differential equations to ordinary one. A computer software-based MATLAB function bvp4c is implemented to handle the envisioned mathematical model. Sketches portraying impacts on velocity, temperature, and concentration versus involving parameters are given and deliberated well. It is witnessed that Darcy-Forchheimer coefficient show an opposite trend on radial velocity and temperature field. It is further perceived that melting parameter and radiation parameter has a retarding effect on temperature profile. Skin friction coefficients (SFC) and local Nusselt number (Nul) are evaluated via graphical illustration. Our results demonstrate that the SFC fall for porosity parameter and Nul is boosted for higher values of melting parameter and is reduced in case of high radiation coefficient.

TABLE OF CONTENTS

LIST OF TABLES

LIST OF FIGURES

NOMENCLATURE

Acronyms

CC	Cattaneo-Christov
CNTs	Carbon nanotubes
HH	Homogeneous-Heterogeneous reactions
SFC	Skin friction coefficient
MHD	Magnetohydrodynamics
MWCNTs	Multi-walled carbon-nanotubes
SWCNTs	Single-walled carbon nanotubes
Nul	Local Nusselt number

Symbols

A	Area of surface
$B(t)$	Strength of Magnetic field
B_f	Body force
B_0	Magnetic induction
B^*	Non-Darcian parameter
A^*, B^*	Chemical species
a, b	Concentrations of chemical species
c	Dimensional constant
$(C_p)_c$	Specific heat of nano-particles
C	Concentration of nano-particles
$(C_p)_f$	Specific heat capacity of fluid
$(C_p)_{nf}$	Specific heat capacity of Nano-fluid
C_s	Heat capacity of solid surface
C_b	Drag force

C_f	Specific heat of the fluid
D_A, D_B	Coefficients of Brownian diffusion
D_m	Mass diffusivity
$\frac{D}{Dt}$	Material time derivative
D_E	Dissipation effects
$\frac{du}{dy}$	Velocity gradient
d	Material's thickness
E	System emissivity
F^*	Forchheimer parameter
F	Local inertia parameter
Ha	Hartmann number
h^*	Convective heat transfer coefficient
k	Thermal conductivity
k^*	Mean absorption coefficient
k_{CNT}	Thermal conductivity of carbon-nanotubes
k_f	Base fluid (water) thermal conductivity
k_{nf}	Thermal conductivity of Nano-fluid
K	Permeability of spongy media
$\sqrt{K}$	Inertial permeability
k_1	Material's conductivity
k_s, k_c	Homogeneous reaction parameter
K_1	Homogeneous reaction parameter
K_2	Heterogeneous reaction parameter
L^*	Strain tensor
L	Latent heat

l	Characteristic length
M	Mass of a substance
Me	Melting heat coefficient
N	Behavior of the fluid
P	Pressure
Pr	Prandtl number
q_{rd}	Radiative heat flux
q^*	Darcy-flux/Darcy-velocity
ΔT	Temperature difference
T_0	Temperature of solid
T_h	Temperature at upper disk
T_m	Temperature at lower disk/Surface temperature
v	Velocity of the fluid
V	Material's volume
(U,V,W)	Components of Velocities
$\theta(\eta)$	Dimensionless temperature
$f'(\eta)$	Radial velocity (Dimensionless velocity)
$f(\eta)$	Axial velocity (Dimensionless velocity)
$h(\eta)$	Dimensionless concentration for homogeneous-reaction
$g(\eta)$	Dimensionless concentration for heterogeneous-reaction
η	Similarity transformation variable
τ_c	Cauchy stress tensor
τ_{yx}	Shear stress normal to the surface in the x-direction
μ_f	Fluid dynamic viscosity
ρ	Density

ρ_p	Density of nano-particles
ρ_{CNT}	Density of carbon-nanotubes
θ_w	Temperature ratio parameter
σ_{nf}	Nano-fluid electrical conductivity
ν_f	Kinematic viscosity of the fluid
σ^*	Stefan Boltzmann constant
γ	Thermal relaxation coefficient
ρ_c	Density of carbon-nanotubes
μ	Dynamic viscosity
μ_{nf}	Nano-fluid dynamic viscosity
ρ_f	Density of fluid
ρ_{nf}	Nano-fluid density
λ	Porosity parameter
ϕ	Volume fraction of nanoparticles
ν	Kinematic viscosity
ν_{nf}	Nano-fluid kinematic viscosity
k^*	Mean absorption coefficient
α	Thermal diffusivity

Subscripts

0	Solid
1	Homogeneous reaction
2	Heterogeneous reaction
c	Carbon-nanotubes
f	Fluid
h	Upper disk

L	Local
m	Melting heat at lower disk
nf	Nano-fluid
p	Constant pressure
r	Radiative heat transfer

Chapter 1

Introduction and literature review

1.1 Introduction

Nano-fluids are solid-liquid compound substances that have an ability to transfer heat beyond a small temperature difference. These fluids acquire metaphysical features such as viscidity, consistency and specific heat etc. for heat transit applications. Adding nano-sized particles in the base fluid *e.g.*, water becomes nano-fluid. These nano-sized particles are called nano-particles and can be form of carbon nanotubes, metals and oxides and consumed to enhance the thermal conductivity and accomplishment of heat transportation. In comparison with conventional fluids, the standard heat transit fluids intrinsically have weak thermal conductivity. Smaller channels would get hindered in case of standard fluids which comprise milimeter or micrometer sorted particles. Advancement of nano-fluids is one of the modern technologies. By dissipating nano-particles less than 100 nm in diameter, nano-fluids are extra ordinary proficient heat transit fluids. Improvement in nano-fluid thermal conductivity plays a vital role in innumerable industrial applications. Having four properties nano-fluids have outstanding characteristics:

- Enhancement of thermal conductivity using low concentration of nano-particles
- Potent temperature dependent thermal-conductivity

- Nonlinear development in thermal-conductivity using nano-particles and
- Augmentation in boiling crucial heat flux.

The existence of homogeneous-heterogeneous reactions plays significant role in chemical reactions. Sometimes, in certain cases the process of chemical reactions is slow. In this case, the existence of a catalyst is must to subdue this perplexity. The interaction amongst homogeneous and heterogeneous reactions is very tangled at distinct rates into the fluid and onto the surface of catalyst in case of manufacturing and depletion of reactant species. some examples are combustion, catalysis, and bio-chemical processes. Carbon nano-tubes (CNTs) are cylindrical-shaped graphene plates. The CNTs are single-walled carbon nano-tubes (SWCNTs) or multi-walled carbon nano-tubes (MWCNTs). The CNTs are expressed as the extraordinary stuffs of the present times due to their advanced physico-chemical appearance, and the thermic and mechanical aspects. Recently, with vast applications in technological and industrial systems squeezed flow amidst two parallel disks has attained great attention. Many devices such as stirring piston in engine, hydraulic brakes, and chocolate filler are based on the flow principle amid squeezing regions. Squeezing flow is involved in nasogastric tubes and syringes with the effect of moving disk. Having the property to change their shape, squeezed flows are expectedly unstable flows.

The first scientific work on thermal radiation was developed by Della-Porta in 16^{th} century. At the end of 18^{th} century, Prevost [1] determined the theory which states that all bodies radiate heat, the greater the temperature the higher the radiation *e.g.*, two bodies with distinct temperatures, the heated body will transfer heat to the colder one till they reach the uniform temperature which is known as Prevost Theory of Exchanges. Afterwards, in the beginning of 19^{th} century Davy and Rumford studied the aspects of thermal radiation. Thermal radiations has many applications in engineeing field, space and in material and mechanical sciences. Radiative heat transfer in many processes such as space vehicle, fossil fuel combustion energy, cosmological flows and in solar energy technology performs a very important role. In flow and heat transfer phenomenon it is of

major interest operating at high temperature in the structure of various innovative energy renovation systems. Effects of thermal radiation play a significant role in case of large difference among the surface and ambient temperature. The phenomenon of melting and liquid freezing over the half-space surface was the work subject of Stefan [2] at the end of 19^{th} century. Melting heat transfer has abundant significance in composition of frozen ground defrosting, laser fabrication, metal molding, magma solidification and storage of thermal energy.

Heat conduction Fourier's law has been a criterion benchmark in many practical applications to estimate the behavior of heat transmission. Nevertheless, in view of parabolic-heat equation due to an initial disorder system suffers alot. Cattaneo [3] tackled this drawback of the Fourier model through addition of thermal time relaxation. Hence, this modification has created the hyperboli-heat equation for temperature field. Also, within finite speed the heat transmisssion is permitted to circulate through thermal-waves. Christov [39] modified Cattaneo's model by introducing thermal relaxation time in terms of Oldroyd's upper-convicted derivative to achieve the material-invariant formulation. Tibullo and Zampoli [4] have worked on innumerable practicable applications *i.e.*, to nano-fluid flow from skin-burn detriment model. Henry Darcy [5] (a civil french engineer) defined the fluid flow over a porous surface based on the outcomes of experiments on the flow of water over cribs of sand, on hydro-geology, in the earth sciences. For the water flow, he studied the aspects of sand filters. After his experiments, he deliberated that viscous forces dominate around inertia forces within spongy media. Afterwards, which become Darcy-law. Darcy-law presumes laminar flow of the fluid in the absence of density (inertia term) which indicates that absence of inertia term is not the case in classical Navier-Stokes equations. An immense surface area in a spongy media is subject to fluid flow which is the innate supposition of Darcy-law.

Darcy-law has tremendous importance in oil estates, ground water structures, petroleum engineering and grain stoke. This is not appropriate nearby the wall because of high flow rates of porous media. Keeping this in mind, one has to become thoughtful

of the non-Darcian impacts by spongy media in the analysis of fluid flow and rate of heat-transfer. Philippe Forchheimer [6] while heat passing throughout coal frame exposed the non-linear relation amongst potential gradient and rate of flow at high amount of velocity. Initially, he concluded that this augmentation in non-linearity is due to turbulance in fluid flow but afterwards it is discovered that this is because of porosity of media. Hence, Forchheimer mechanism was determined for high flow rate. This was the modification in Darcy-law with addition of quadratic term in equation of motion and this modifcation is called Darcy-Forchheimer statement. For higher Reynolds number, it was termed as Darcy-Forchhimer term by Muskat [7]. Substantially, for higher filteration velocities a quadratic drag appears in equation of motion for porous media. Because of solid obstructs, this drag is poduced and at the surface it becomes identical with surface drag through resistance. There are countless examples of finite situations where these inertia effects are considerable with no use of Darcy-law. Hence, Darcy-Forchheimer law has a vital role in the fluid flow with high velocity.

1.2 Literature review

Having astonishing heat-transit characteristics in contrast with usual heat transit fluids, nano-fluids with extraordinary heat transit characteristics is the most discoursed subject of present time [8-9]. In universal heat transit fluids *e.g.*, water, oil, and ethylene glycol etc. Nano-fluids contain nanoparticles with size under 100nm. Sensational advancement in the thermal effects of host fluids is produced when a very slight quantity of nanoparticles suspended thoroughly and dissipates constantly in the base fluids. To create steady and highly conducted nano-fluids one step and two step methods are used but creating nano-particles both methods endure cluster of nanoparticles. This is the crucial issue in industrial science including nano-powder. The solution over cluster of nanoparticles is to dissipate mono-sized nanoparticles to produce extra-ordinary steady nano-fluid is studied by Uddin et al. [10]. Sheikholeslami et al. [11] reported the squeezing nano-fluid

fluctuating flow amid two parallel surfaces by Adomian-Decomposition-method (A-D-M). Mittal and Pandit [12] investigated first time flow of squeezing nano-fluid fluctuating flow amid two parallel surfaces with wavelets. A significant study over nano-fluid flow has been deliberated by Ramzan et al. [13]. Some recent explorations regarding nano-fluids are given at [14-17].

Carbon nano-tube is a large stretched, thin and cylinder-shaped molecule of pure carbon, around 1 to 3 nano-meters (1 to 3 billionth of a meter) in breadth (diameter), and 100 to 1000s of nano-meters long. Iijima [18] introduced the theory of carbon-nanotubes. CNTs are classified in SWCNTs and MWCNTs based on structure with wide applications *i.e.*, flat-panel displays, conductive plastics, radar-enthralling covering, antifouling paint, technical textiles, gas stowage, micro and nanoelectronics etc. Having high compatibility with biomolecules like purification of contaminated drinking water, DNA and for proteins, CNTs are accustomed in biosensors and medical appliances [19]. Hayat et al. [20] studied the squeezing flow of CNTs amidst two parallel disks on Darcy-Forchheimer porous media. It is concluded that the temperature increases with high nanoparticle volume fraction.

Stefan [21] proposed the idea of squeezing flow in 1874. Afterwards, many researchers explored the problems regarding squeezing flow. The theoretical investigation regarding squeezing flow amid parallel disks is presented by Leider and Bird [22]. Qayyum et al. [23] discussed the time-dependent squeezing Jeffery fluid flow amid two parallel disks. Haq et al. [24] scrutinized the MHD nano-fluid squeezed flow based on water with carbon nanotubes amidst two-parallel disks. It is concluded that temperature and velocity profiles increase with high nanoparticle volume fraction. Hayat et al. [25] discussed about squeezed nano-fluid flow-based carbon-nanotubes with impacts of thermal radiations on Darcy-Forchheimer spongy media. He deliberated that an augmentation in nanoparticle volume fraction causes reduction in both velocity and temperature of the fluid. Hashmi et al. [26] investigated the analytical simulations for squeezing nano-fluid flow amidst parallel disks. Analytic simulations for heat transfer and squeezing flow past a spongy

surface are obtained by Mehmood et al. [27].

Henry Darcy [5] defined the fluid flow over a spongy surface based on the outcomes of water flow experiments over cribs of sand and on hydro-geology. He first defined his idea of fluid flow over a spongy media in 1856. Later, due to its limitations of small velocity with weaker permeability, this perception couldn't get fame. Afterward, Philipps Forchheimer [6] modified the momentum equation by velocity square within Darcian velocity. This was afterwards known as Forchheimer term designated by Muskat [7]. Hayat et al. [28] scrutinized squeezing carbon-nanotubes based on water with thermal radiations over a Darcy-Forchheimer spongy media. He deliberated that velocity and temperature fall with increase in nanoparticle volume fraction and temperature increases with increment in Darcy-Forchheimer number. Jha and Kaurangini [29] presented the analytic solutions for Darcy-Forchheimer based spongy media relation. Nasir et al. [30] investigated 3D Darcy-Frocheimer thermal radiative flow of SWCNTs with generation and absorption of convective heat along a rotating stretchable disk. It is found that velocity falls with higher Darcy-Forchheimer number and temperature augments with high estimates of radiation parameter. Khan et al. [31] discussed the influences of HH reactions for Darcy-Forchheimer flow. It is found that velocity reduces for higher estimates of Darcy-Fochheimer number. Hayat et al. [32] reported the MHD nano-fluid flow against thermal radiations with partial slip. He concluded that rate of heat transfer increases with rise in radiation parameter. Mukhopad-hyay [33] examined the impact of thermal radiation in MHD flow by exponential stretchable spongy surface. Sheikholeslami et al. [34] investigated the MHD nano-fluid flow with impacts of thermal radiations, thermophoresis and Brownian motion parallel rotating disks. It is concluded that with high thermal radiation concentration boundary layer thickness reduces. Mohyud-Din et al. [35] scrutinized the effects of nonlinear thermal radiations on squeezing Casson fluid flow amidst parallel disks. He deliberated that radiation parameter has a retarding impact on temperature profile. Epstein and Cho [36] studied the time-independent laminar flow with melting heat transfer past a stationary plate. Hayat et al. [37] investigated the

melting heat transfer effects with HH reactions in the fluid flow within CNTs. It is concluded that melting parameter has reverse impact on fluid temperature and velocity. Krishnamurthy et al. [38] scrutinized the impacts melting heat transfer with chemical reaction of Williamson nano-fluid in spongy media. It is found that velocity increases whereas temperature decreases due to high estimates of melting parameter. Christov [39] studied on modification of Maxwell-Cattaneo model which is known as CC thermal flux model. The analytic solution of visco-elastic in the existence of CC thermal flux and velocity-slip edge were investigated by Han et al. [40]. The influence of CC heat flux fluid flow containing nanotubes is scrutinized by Lu et al. [41]. Ramzan et al. [42] scrutinized the third-grade fluid flow with HH reactions in the existence of CC heat flux. Lu et al. [43] discussed the mathematical-model of unsteady fluid flow containing SWCNTs and MWCNTs in the presence of CC heat flux and HH reactions amidst two parallel disks.

From the aforesaid discussion, it is perceived that there is no such study with combined influences of melting heat transfer, non-linear thermal radiation, CC heat flux and HH reactions on Darcy-Forchheimer porous media amidst parallel disks. Comparably, less research work with carbon-nanotubes is done. So, the current analysis is to inspect the melting heat transfer effects in the carbon nanotubes based nanofluid flow in a nonlinear Darcy-Forchheimer porous media amidst two parallel disks with CC heat flux and HH reactions. Impacts of prominent parameters on SFC and Nul are portrayed via graphic illustration. Numerical solution of present work is obtained by adopting bvp4c built-in function of MATLAB scheme.

Chapter 2

Preliminaries

This chapter is consists of certain perceptions, definitions and fundamental laws.

2.1 Fluid

A substance that can stream under an influence of shear force continuously is called fluid. Some fundamental examples are water, oil, and blood etc.

2.2 Nanofluid

A fluid which consists of nanoparticles which are made of carbon nano-tubes, metals or oxides is called nanofluid. These nanoparticles of the fluid are basically used to enhance the tranfer of heat and the thermal conductivity of fluid.

2.3 Fluid mechanics

It is the form of science which deals with the characteristics of all type of fluid bahaviour *i.e.*, in rest or movement. Fluid mechanics is categorized into two classes:

2.3.1 Fluid statics

This class of fluid mechanics belongs to the study of fluid characteristics at rest.

2.3.2 Fluid Dynamics

This class of fluid mechanics belongs to the study of fluid characteristics in the state of motion.

2.4 Flow

It is specified as a subtance that continually deforms fluently under the effects of distinct form of forces. Flow is further categorised into two classess:

2.4.1 Laminar flow

It is a kind of flow in which velocity is unchanged at each level and fluid flow is in uniform state.

2.4.2 Turbulent flow

It is a kind of flow in which velocity changes at each level and fluid flow moves randomly.

2.5 Squeezed flow

A flow between two parallel or approximately parallel boundaries impending each other in which a material is deformed, is called a squeezed flow. Having the property to change their shape, squeezed flows are expectedly unstable and discordant flows.

2.6 Viscosity

It is the attribute of fluid which estimates the resistant force of fluid flow over deformation when innumerable forces are acting on the fluid. It can be classified into two ways:

2.6.1 Dynamic viscosity (μ)

It is the measure of resistivity of fuild flow. Mathematically, it can be expressed as:

$$\mu = \frac{\text{Shear stress}}{\text{Gradient of velocity}}, \tag{2.1}$$

or

$$\mu = \frac{\tau_{yx}}{(du/dy)}. \tag{2.2}$$

In units of system international, unit of μ is $\frac{\text{kilogram}}{\text{meter.sec}}$ with dimension $[M/LT]$.

2.6.2 Kinematic viscosity (ν)

It is precised as the rate of dynamic viscosity (μ) to the fluid density (ρ). Mathematically, it can be displayed as:

$$\nu = \frac{\text{Dynamic viscosity}}{\text{Fluid density}} = \frac{\mu}{\rho}. \tag{2.3}$$

Unit of kinematic viscosity ν is $\frac{\text{meter}^2}{\text{sec}}$ with dimension $[L^2/T]$.

2.7 Newton's law of viscosity

Fluids which demonstrate the continuous and direct relation amid shear stress and gradient of velocity. Mathematically, expression for Newton's law can be represented as:

$$\tau_{yx} \propto (du/dy)\,, \tag{2.4}$$

or

$$\tau_{yx} = (\mu)\,(du/dy)\,. \tag{2.5}$$

2.7.1 Newtonian fluids

A fluid which obeys the Newton's law of viscosity is called Newtonian fluid. In this fluid, a linear relation is found among τ_{yx} and $\frac{du}{dy}$. Some fundamental examples are water, oil, solutions of sugar, glycerin and alcohol etc.

2.7.2 Non-Newtonian fluids

A fluid which does not obey the Newton's law of viscosity is called Newtonian fluid. In this type of fluid, relation among τ_{yx} and $\frac{du}{dy}$ is not linear. Mathematically,

$$\tau_{yx} \propto (du/dy)^N\,, \qquad N \neq 1, \tag{2.6}$$

or

$$\tau_{yx} = (K)\,(du/dy)^N\,. \tag{2.7}$$

Above expression is changed into Newton's law of viscosity ($Eq.$ 2.5) when $K = \mu$ and $N = 1$ $i.e.$,

$$\tau_{yx} = (\mu)\,(du/dy)\,, \qquad \mu = (K)\,(du/dy)^{N-1}\,. \tag{2.8}$$

Fluids like honey, katchup, flour show the conduct of non-Newtonian fluids.

2.8 Density

It is ratio of mass of a subtance to its volume. Density is used to find how much matter of a subtance is present in unit volume. Mathematically,

$$\rho = (M/V)\,. \tag{2.9}$$

Its unit in SI system is $\frac{\text{kilogram}}{\text{meter}^3}$.

2.9 Pressure

It is the ratio of force applied (F_n) normal to the surface area (A). Mathematically,

$$P = (F_n\ /A)\,. \tag{2.10}$$

Its unit in SI system is $\frac{\text{Newton}}{\text{meter}^2}$.

2.10 Magnetohydrodynamics

It is the combination of three words magneto (magnetic), hydro (water) and dynamic (motion of an object under some force) which explains the magnetic impacts of fluid under electric conduction.

2.11 Heat flux

It is the energy transmission per unit time and area. It is also known as thermal flux. Mathematically,

$$Q = (-kA)\,(\nabla T)\,, \tag{2.11}$$

or

$$q = -k\,(\nabla T)\,, \tag{2.12}$$

which is called one-dim Fourier's law. Its unit in S-I is $\frac{\text{watts}}{\text{square meter}}$.

2.12 Cattaneo-Christov heat flux

It is the modification of Fourier's law by two scientists Cattaneo [3] and Christov [39]. Mathematically,

$$q + \varepsilon \left[\frac{\partial q}{\partial t} + V.\nabla q - q.\nabla V + (\nabla .V)\, q \right] = -k\nabla T. \tag{2.13}$$

2.13 Chemical reactions

2.13.1 Homogeneous reaction

A reaction in which proportions remain unchanged throughout the whole process or a reaction which occurs in a one phase is called a homogeneous reaction. Some physical examples are air, vinegar, dishwashing liquid, sugar water and rain.

2.13.2 Heterogeneous reaction

A reaction in which proportions vary throughout the whole process or a reaction which occurs in more than one phases is called a heterogeneous reaction. Some physical examples are earth's atmosphere, mixture of sand and water, sand and sugar etc.

2.14 Porous surface

A surface which consists of holes authorizes the exterior stuff to pass through it. Some examples of porous surfarce are sponge, fabric, card board etc. Rocks, tissues and cork are some biological examples of porous surface.

2.15 Porosity

It is the attribute of spongy surface being full of small pores.

2.16 Permeability

It is the intensity of spongy material which authorizes the fluid to migrate through it. The materials having large holes are highly permeable.

2.17 Mechanism of heat flow

A form of energy transport from hotter to colder systems. It takes place among those subjects having distinct coditions *i.e.*, temperature. This transit of heat takes place through three techniques, covection, radiation and conduction.

2.17.1 Conduction

In this mechanism of heat transit, heat flows from hot to cool surface due to the collisions of unconditional molecules and electrons in solids and liquids. In mathematical form,

$$Q = -kA\nabla T = -kA\left(\frac{dt}{dx}\right), \tag{2.14}$$

here, negative sign is denoting the flow from higher to lower area.

2.17.2 Convection

In this heat transit mechanism, heat flows from hot to cool surface due to the collisions of unconditional molecules and electrons in gasses and liquids. In mathematical form,

$$Q = HA\left(T_{sys} - T_{inf}\right). \tag{2.15}$$

2.17.3 Radiation

In this mechanism of heat transit, heat flows through hot to cold surface by means of electromagnetic tides. Mathematically,

$$Q = E\sigma^* A\left(\Delta T^4\right), \tag{2.16}$$

or

$$Q = E\sigma^* A\left(T_1^4 - T_2^4\right), \tag{2.17}$$

or

$$Q = -E\sigma^* A\left(T_2^4 - T_1^4\right), \tag{2.18}$$

or

$$q = \frac{Q}{A} = -E\sigma^*\left(T_2^4 - T_1^4\right). \tag{2.19}$$

Some physical examples are ultraviolet light from the sun, microwaves from a microwave oven and visible light from a candle etc.

2.18 Darcy law

Darcy law states that heat is directly proportional to the permeability of porous medium K^*, cross-sectional area A, pressure drop ΔP and is inversely proportional to the dynamic viscosity μ.

$$Q = -\frac{K^* A}{\mu}\left(\Delta P\right), \tag{2.20}$$

or

$$\Delta P = P_2 - P_1 = -\left(\frac{Q}{A}\right)\frac{\mu}{K^*}, \tag{2.21}$$

or

$$\Delta P = -\frac{\mu}{K^*} q. \tag{2.22}$$

In case of fluid flow $q = v$ (velocity of fluid):

$$\Delta P = -\frac{\mu}{K^*} v. \tag{2.23}$$

Negative sign is due to the direction of fluid/heat flow from high pressure region to low pressure region.

2.19 Darcy-Forchheimer law

The fluid flow through a porous saurface with Reynolds number greater than 10 and inertial effects in Darcy-law is called Darcy-Forchheimer law. This additive term (inertial effects/velocity square term) is called Forchheimer term which depicts the non-linear conduct of pressure difference against data flow. Mathematically,

$$\frac{\partial P}{\partial X} = -\frac{\mu}{K} v - \frac{\rho_f C_b}{\sqrt{K}} v^2. \tag{2.24}$$

In case of heat flow through cross sectional area:

$$\frac{\partial P}{\partial X} = -\frac{\mu}{K} q^* - \frac{\rho_f C_b}{\sqrt{K}} q^{*2} \ . \tag{2.25}$$

2.20 Melting heat

It is a physical operation in which substance converted to liquids from solids and phase modulation occurs with an increment in internal energy. The substance temperature augments at a melting stage while viscosity decreases. Mathematically,

$$k_{nf} \left(\frac{\partial T}{\partial Z} \right)_{Z=0} = \rho_{nf} \left(C_s \left(T_m - T_0 \right) + L \right) W \left(R, 0 \right). \tag{2.26}$$

2.21 Latent heat

It is the amount of heat per unit mass required to change a solid into a liquid (*i.e.*, ice into water and water into steam etc.) with constant temperature. Mathematically,

$$L = \frac{Q}{M}. \tag{2.27}$$

2.22 Non-dimensional parameters

2.22.1 Skin friction coefficient (C_{fr})

It is the amount of drag force faced by the fluid while passing through the surface. It takes place amogst the liquid and intense surface which reduces the rate of fluids flow. Mathematically, it can be written as:

$$C_{fr} = \frac{\tau_s}{\frac{1}{2}\rho v^2}. \tag{2.28}$$

2.22.2 Nusselt number (Nu)

It is the dimensionless amount which describes the relation amongst conduction and convection heat transit parameters along the boundary. In mathematical form

$$N_L = \frac{h^* \Delta T}{(k\Delta T\ /l)} = \left(\frac{h^* l}{k}\right). \tag{2.29}$$

2.22.3 Prandtl number (Pr)

It is the ratio of momentum diffusivity to the thermal diffusivity.

$$Pr = (\nu/\alpha) = (\mu C_p/k). \tag{2.30}$$

2.22.4 Hartmann number (Ha)

It describes the relationship amongst induced frictional force (through magnetism) and viscosity. It is the ratio of magnetic to the viscous forces. Mathematically,

$$Ha = \sqrt{\frac{B_0^2 L^2 r^*}{\mu}}. \tag{2.31}$$

2.22.5 Reynolds number (Re)

It is the dimensionless number which is used to acknowledge the type of fluid whether it is laminar or turbulent. It is the rate of inertial and viscous forces. Mathematically,

$$Re = \frac{\text{Inertial forces}}{\text{viscous forces}} = (vl/\nu)\,. \tag{2.32}$$

This number is used to differentiate flow behavior *i.e.*, laminar or turbulent. At lower Reynolds number, laminar flow appears in which viscous impacts are promonent while turbulent flow appears at large value of Reynolds number in which inertial impacts are prominent.

2.22.6 Radiation parameter (R_d)

It is the relative assistance of conduction to the transmission of thermal radiation. Mathematically,

$$R_d = \frac{16\sigma^* T_m^3}{3k_f k^*}. \tag{2.33}$$

2.22.7 Thermal relaxation parameter (γ)

It is the dimensionless parameter which is used to evaluate the time needed for conduction of heat. It describes the time which is occupied for a hot material to rescue its 50 percent heat beacause of diffusion.

2.22.8 Schmidt number (Sc)

It is the rate of viscosity (Kinematic) to mass diffusivity. Mathematically,

$$Sc = (\nu/D_m)\,. \tag{2.34}$$

2.22.9 Forchheimer number (F)

It is the rate of pressure gradient to viscous resistivity and can be represented mathematically as:

$$F = \frac{K\rho v B^*}{\mu}. \tag{2.35}$$

2.22.10 Melting parameter (Me)

It is the dimensionless quantity which is compound of two stefan quantities $\left(\frac{c_f\left(T_{inf}-T_m\right)}{\lambda}\right)$ and $\left(\frac{c_f(T_m-T_0)}{\lambda}\right)$ in case of solid and liquid facets. Mathematically,

$$Me = \frac{C_f\left(T_{inf}-T_m\right)}{L + C_s\left(T_m - T_0\right)}. \tag{2.36}$$

2.23 Thermal conductivity (k)

Thermal conductivity is the measure of the material's capacity to conductive heat. It is the conductive heat Forier's law which is the rate of the product of heat transit amount (Q) and meterial's thickness (d) to the area (A) and temperature difference (ΔT). Mathematically,

$$k = \frac{Qd}{A\Delta T}\ , \tag{2.37}$$

or

$$k = q\frac{d}{\Delta T}, \tag{2.38}$$

with unit (W/mK).

2.24 Conservation laws

A significant measure which remains uniform in an solitary system with the time progression is known as conserved quantity. The law that deals with the conserved quantity is called conservation law. Some fundamental conservative laws are as follows:

2.24.1 Mass conservation law

In this law the entire mass remains conserved in any closed system. Mathematically,

$$\frac{D\rho}{Dt} + \rho\left(\nabla.\mathrm{V}\right) = 0, \tag{2.39}$$

or

$$\frac{\partial\rho}{\partial t} + \left(\mathrm{V}.\nabla\right)\rho + \rho\left(\nabla.\mathrm{V}\right) = 0, \tag{2.40}$$

or

$$\frac{\partial\rho}{\partial t} + \nabla.\left(\rho\mathrm{V}\right) = 0, \tag{2.41}$$

which is called continuity equation. In case of steady flow *i.e.*, (ρ = constant), the above equation becomes

$$\nabla.\left(\rho\mathrm{V}\right) = 0, \tag{2.42}$$

while for an incompressible flow

$$(\nabla.\mathrm{V}) = 0. \tag{2.43}$$

2.24.2 Momentum conservation law

In this law total linear momentum remains unchnaged in a closed system. Mathematically,

$$\rho\frac{D\mathrm{V}}{Dt} = \mathrm{div}\ \tau_c + \rho B_f, \tag{2.44}$$

with,

$$\tau_c = -PI + \mu A_1. \tag{2.45}$$

2.24.3 Energy conservation law

In this law whole energy in any closed system remains conserved. Mathematically,

$$(\rho C_p)_f \frac{DT}{Dt} = \tau_c.\acute{L} - \mathrm{div}\, q + \rho D_E, \tag{2.46}$$

where q and $\acute{L}$ are:

$$q = -k\nabla T, \tag{2.47}$$

$$\acute{L} = \nabla V, \tag{2.48}$$

and for this law τ_c is:

$$\tau_c = -pI + \mu A_1, \tag{2.49}$$

$$A_1 = \acute{L} + \acute{L}^T. \tag{2.50}$$

2.24.4 Concentration conservation law

The volume division or fraction equation (by using principle of mass-conservation) for nano-particles is:

$$\frac{\partial C}{\partial t} + \ (\mathrm{V}.\nabla)\, C = -\frac{1}{\rho_p}\,(\nabla . J_p)\,. \tag{2.51}$$

Fick's law of mass diffusion is

$$J_p = -\rho_p D_m \nabla C. \tag{2.52}$$

Following above law, we get

$$\frac{\partial C}{\partial t} + (\mathrm{V}.\nabla)\, C = D_m \nabla^2 C. \tag{2.53}$$

2.25 Thermal diffusivity (α)

It is the rate of thermal conductivity to density and specific heat capacity which is used to characterize the time-dependent fluid cunductive heat flow. This dimensionless parameter tells us how promptly a substance react with temperature modification. In mathematical form

$$\alpha = \frac{k}{\rho C_p}\ . \tag{2.54}$$

Chapter 3

Unsteady squeezing carbon nanotubes based Nano-liquid flow with Cattaneo-Christov heat flux and homogeneous-heterogeneous reactions

In this chapter, unsteady flow of squeezing nano-fluid water-based single-walled (SW) & multi-walled (MW) carbon nano-tubes (CNTs) amidst two parallel disks with effects of Cattaneo-Christov heat flux and homogeneous-heterogeneous reactions is discussed. In addition to above, the impact of magnetohydrodynamics (MHD) is also considered. The requisite boundary layer equations are transformed into non-linear ordinary differential equations after using appropriate similarity-transformation. The obtained system of equations is addressed by bvp4c built-in function of MATLAB scheme. The outcomes of the prominent parameters versus involved profiles are portrayed and conversed in the light of their physical significance. This is review work of [43].

3.1 Mathematical formulation

We consider a time dependent, incompressible 2D-magnetohydrodynamic (water-based) nano-particle fluid flow amidst 2-infinite parallel disks by the length Z, where Z is defined as:

$$Z = h(t) = H(1 - ct)^{0.5}. \tag{3.1}$$

We have considered two types of nano-particles, SWCNTs and MWCNTs, along the base fluid (water) with suction case only ($W_0 \gtrsim 0$). Furthermore, direction of magnetic field is normal to the disks. By considering small Reynolds number, the induced magnetic field is not taken into consideration. Here, temperature T_h indicates the upper disk temperature and Temperature T_w indicates the lower disk $Z = 0$. Moreover, the upper disk at $Z = h(t)$ is moving to and fro with the velocity $\frac{dZ}{dt}$ from the immobile and porous lower disk at $Z = 0$. We have considered the cylindrical coordinate system (R, α, Z) and the velocity component V vanishes identically due to rotational flow symmetry $\left(\frac{\partial}{\partial \alpha} = 0\right)$. The direction of flow is vertically upward towards the $Z - axis$.

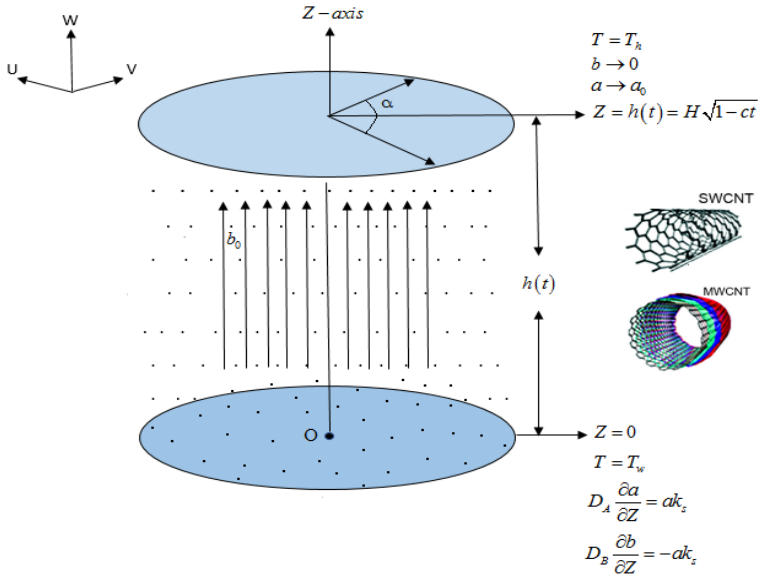

Figure 3.1 Fluid geometry

Chaudhary and Merkin [44] designed a homo-geneous (isothermic-cubical-autocatalytic) and hetero-geneous chemical reactions along 2-chemical species A^* and B^* such that,

$$A^* + 2B^* \rightarrow 3B^*, \qquad \text{rate} = k_c a b^2, \tag{3.2}$$

$$A^* \rightarrow B^*, \qquad \text{rate} = k_s a. \tag{3.3}$$

Here, concentrations for these chemical species are expressed by a, b and k_j, with $(j = c, s)$ where a, b and k_j are rate quantities. These reactions are presumed to be an isothermic.

For incompressible fluid density is constant. The equations of conservation of mass, momentum, energy and concentration are as follows:

$$\boldsymbol{\nabla}.\mathbf{V} = \mathbf{0}, \tag{3.4}$$

$$\rho_{nf}\frac{\mathbf{dV}}{\mathbf{dt}} = -\boldsymbol{\nabla}\mathbf{P} + \mu_{nf}\boldsymbol{\nabla}^2\mathbf{V} + \rho_{nf}\sigma\left(\mathbf{J}\times\mathbf{B}\right), \tag{3.5}$$

$$\left(\rho C_p\right)_{nf}\frac{\mathbf{dT}}{\mathbf{dt}} = -\boldsymbol{\nabla}.\mathbf{q}, \tag{3.6}$$

where $\mathbf{q}$ is Cattaneo-Christov heat flux for incompressible fluid given as:

$$\mathbf{q} + \boldsymbol{\epsilon}\left(\mathbf{V}.\boldsymbol{\nabla}\mathbf{q} - \mathbf{q}.\boldsymbol{\nabla}\mathbf{V}\right) = -k_{nf}\nabla\mathbf{T}. \tag{3.7}$$

Taking $\boldsymbol{\nabla}$ on both sides of Equation (3.7) and using Equation (3.6), we get

$$\mathbf{T}_t + \mathbf{V}.\boldsymbol{\nabla}\mathbf{T} + \boldsymbol{\epsilon}\left[\mathbf{T}_{tt} + 2\mathbf{V}.\boldsymbol{\nabla}\mathbf{T}_t + \mathbf{V}_t.\nabla\mathbf{T} + \mathbf{V}.\boldsymbol{\nabla}\left(\mathbf{V}.\boldsymbol{\nabla}\mathbf{T}\right)\right] = \frac{k_{nf}}{\left(\rho C_p\right)_{nf}}\boldsymbol{\nabla}.\left(\boldsymbol{\nabla}\mathbf{T}\right), \tag{3.8}$$

$$\frac{\mathbf{d}a}{\mathbf{dt}} = D_A\left(\boldsymbol{\nabla}^2 a\right) - k_c a b^2, \tag{3.9}$$

$$\frac{\mathbf{d}b}{\mathbf{dt}} = D_B\left(\boldsymbol{\nabla}^2 b\right) + k_c a b^2. \tag{3.10}$$

The governing equations from Equations $(3.4) - (3.5)$ and $(3.8) - (3.10)$ are represented

as

$$\frac{\partial U}{\partial R}+\frac{U}{R}+\frac{\partial W}{\partial Z}=0, \tag{3.11}$$

$$\frac{\partial U}{\partial t}+U\frac{\partial U}{\partial R}+W\frac{\partial U}{\partial Z}=-\frac{1}{\rho_{nf}}\frac{\partial P}{\partial R}+\frac{\mu_{nf}}{\rho_{nf}}\left(\frac{\partial^2 U}{\partial R^2}+\frac{1}{R}\frac{\partial U}{\partial R}-\frac{U}{R^2}+\frac{\partial^2 U}{\partial Z^2}\right)-\sigma B^2(t)U, \tag{3.12}$$

$$\frac{\partial W}{\partial t}+U\frac{\partial W}{\partial R}+W\frac{\partial W}{\partial Z}=-\frac{1}{\rho_{nf}}\frac{\partial P}{\partial Z}+\frac{\mu_{nf}}{\rho_{nf}}\left(\frac{\partial^2 W}{\partial R^2}+\frac{1}{R}\frac{\partial W}{\partial R}+\frac{\partial^2 W}{\partial Z^2}\right), \tag{3.13}$$

$$\begin{aligned}\frac{\partial T}{\partial t}+U\frac{\partial T}{\partial R}+W\frac{\partial T}{\partial Z}+\varepsilon&\begin{pmatrix}\frac{\partial^2 T}{\partial t^2}+\frac{\partial U}{\partial t}\frac{\partial T}{\partial R}+2U\frac{\partial^2 T}{\partial t\partial R}\\ +2W\frac{\partial^2 T}{\partial t\partial Z}+\frac{\partial W}{\partial t}\frac{\partial T}{\partial Z}+U\frac{\partial U}{\partial R}\frac{\partial T}{\partial R}\\ +W\frac{\partial W}{\partial Z}\frac{\partial T}{\partial Z}+U\frac{\partial W}{\partial R}\frac{\partial T}{\partial Z}+W\frac{\partial U}{\partial Z}\frac{\partial T}{\partial R}\\ +2UW\frac{\partial^2 T}{\partial R\partial Z}+U^2\frac{\partial^2 T}{\partial R^2}+W^2\frac{\partial^2 T}{\partial Z^2}\end{pmatrix}\\ &=\frac{k_{nf}}{(\rho C_p)_{nf}}\left(\frac{\partial^2 T}{\partial R^2}+\frac{1}{R}\frac{\partial T}{\partial R}+\frac{\partial^2 T}{\partial Z^2}\right),\end{aligned} \tag{3.14}$$

$$\frac{\partial a}{\partial t}+U\frac{\partial a}{\partial R}+W\frac{\partial a}{\partial Z}=D_A\left(\frac{\partial^2 a}{\partial R^2}+\frac{1}{R}\frac{\partial a}{\partial R}+\frac{\partial^2 a}{\partial Z^2}\right)-k_c ab^2, \tag{3.15}$$

$$\frac{\partial b}{\partial t}+U\frac{\partial b}{\partial R}+W\frac{\partial b}{\partial Z}=D_B\left(\frac{\partial^2 b}{\partial R^2}+\frac{1}{R}\frac{\partial b}{\partial R}+\frac{\partial^2 b}{\partial Z^2}\right)+k_c ab^2. \tag{3.16}$$

Here, D_A and D_B are the diffusion coefficients. The suitable boundary conditions are described as:

$$U=0, \qquad W=-\frac{W_0}{(1-ct)^{\frac{1}{2}}}, \qquad T=T_w, \qquad D_A\frac{\partial a}{\partial Z}=k_s a,$$

$$D_B\frac{\partial b}{\partial Z}=-k_s a, \qquad \text{at} \quad Z=0,$$

$$U = 0, \qquad W = \frac{dh}{dt}, \qquad T = T_h, \qquad a \to a_0, \qquad b \to 0, \qquad \text{at} \;\; Z = h\,(t)\,. \tag{3.17}$$

The thermophysical properties are

$$\mu_{nf} = \frac{\mu_f}{(1-\phi)^{2.5}}, \qquad \nu_{nf} = \frac{\mu_{nf}}{\rho_{nf}}, \qquad \rho_{nf} = (1-\phi)\,\rho_f + \phi\rho_{CNT},$$

$$\frac{k_{nf}}{k_f} = \frac{(1-\phi) + 2\phi\frac{k_{CNT}}{k_{CNT}-k_f}\ln\frac{k_{CNT}+k_f}{2k_f}}{(1-\phi) + 2\phi\frac{k_{CNT}}{k_{CNT}-k_f}\ln\frac{k_{CNT}+k_f}{2k_f}}\,. \tag{3.18}$$

Table 3.1 shows the thermophysical features ρ (density), C_p (specific heat), k (thermal conductivity) of water (Base-fluid) and carbon-nanotubes.

Table 3.1 Physical properties of water (base-fluid), SWCNTs and MWCNTs [45].

Thermophysical traits	Water (Base-fluid)	Nano-particle $(SWCNTs)$	Nano-particle $(MWCNTs)$
$C_p\,(J/kgK)$	4179.00	425	796
$\rho\,(kg/m^3)$	997.100	2600	1600
$k\,(W/kgK)$	0.61300	6600	3000

3.1.1 Similarity transformations

Non-dimensional transformations is defined as:

$$U = \frac{cR}{2(1-ct)}f'(\eta), \qquad W = -\frac{cH}{\sqrt{(1-ct)}}f\,(\eta)\,, \qquad \eta = \frac{Z}{H\sqrt{1-ct}},$$

$$B\,(t) = \frac{B_0}{\sqrt{1-ct}}, \qquad h\,(\eta) = \frac{a}{a_0}, \qquad g\,(\eta) = \frac{b}{a_0}, \qquad \theta\,(\eta) = \frac{T-T_h}{T_w-T_h}. \tag{3.19}$$

Using above tranformations, incompressibilty condition is satisfied and Equations (3.12) − (3.16) are transformed as:

$$\frac{1}{(1-\phi)^{2.5}} f''''(\eta) - Sq\left((1-\phi)+\phi\frac{\rho_c}{\rho_f}\right)$$

$$\left(\begin{array}{c} \eta f'''(\eta)+3f''(\eta) \\ -2f(\eta) f''(\eta) \end{array}\right) - Haf''(\eta) = 0, \tag{3.20}$$

$$\frac{k_{nf}}{k_f}\theta''(\eta) + Sq\,\mathrm{Pr}\left((1-\phi)+\phi\frac{(\rho Cp)_c}{(\rho C_p)_f}\right)$$

$$\left(\begin{array}{c} 2f(\eta)\theta'(\eta) - \eta\theta'(\eta) \\ -\gamma\left(\begin{array}{c} \eta^2\theta''(\eta) - 2\eta f(\eta)\theta''(\eta) - \eta f'(\eta)\theta'(\eta) \\ +f(\eta) f'(\eta)\theta'(\eta) + f^2(\eta)\theta''(\eta) \end{array}\right) \end{array}\right) = 0, \tag{3.21}$$

$$\frac{1}{Sc}h''(\eta) - \frac{\eta}{2}h'(\eta) + f(\eta)h'(\eta) - k_1 h(\eta) g^2(\eta) = 0, \tag{3.22}$$

$$\frac{\delta}{Sc}g''(\eta) - \frac{\eta}{2}g'(\eta) + f(\eta)g'(\eta) + k_1 h(\eta) g^2(\eta) = 0, \tag{3.23}$$

with boundary conditions

$$f(0) = s, \qquad f'(0) = 0, \qquad \theta(0) = 1, \qquad \delta g'(0) = -k_2 h(0),$$

$$h'(0) = k_2 h(0), \qquad \text{at} \quad \eta = 0, \tag{3.24}$$

$$f(1) = \frac{1}{2}, \qquad f'(1) = 0, \qquad \theta(1) = 0, \qquad g(1) \to 0,$$

$$h(1) \to 1, \qquad \text{at} \quad \eta = 1. \tag{3.25}$$

Here

$$\delta = \frac{D_B}{D_A}. \tag{3.26}$$

From Equations (3.2) and (3.3), chemical species A^* and B^* cannot be analogous, but both can be identical in volume. However, presuming that diffusion species D_B and D_A are identical ($\delta = 1$), we have

$$h(\eta) + g(\eta) = 1. \tag{3.27}$$

Using above property, Equations (3.22) and (3.23) take the form

$$\frac{1}{Sc}h''(\eta) - \frac{\eta}{2}h'(\eta) + f(\eta)h'(\eta) - k_1 h(\eta)(1 - h(\eta))^2 = 0, \tag{3.28}$$

with boundary conditions

$$h'(0) = k_2 h(0), \qquad \text{at} \quad \eta = 0, \tag{3.29}$$

$$h(1) \to 1, \qquad \text{at} \quad \eta = 1. \tag{3.30}$$

Here

$$\gamma = \frac{\epsilon c}{2(1-ct)}, \quad Sc = \frac{cH^2}{D_A}, \quad k_1 = \frac{k_c a_0^2 (1-ct)}{c}, \quad k_2 = \frac{k_s}{D_A} H (1-ct)^{\frac{1}{2}},$$

$$Sq = \frac{cH^2}{2\nu_{nf}}, \quad Ha = \left(\frac{\sigma_f B_0^2 H^2}{\mu_f}\right)^{\frac{1}{2}}, \quad \Pr = \frac{\mu C_p}{k_f}, \quad s = \frac{W_0}{cH}. \tag{3.31}$$

SFC and Nul are calssified as:

$$C_{fr} = \frac{\mu_{nf}\left(\frac{\partial U}{\partial Z} + \frac{\partial W}{\partial R}\right)_{Z=h(t)}}{\frac{1}{2}\rho_{nf}\left(-\frac{cH}{(1-ct)^{\frac{1}{2}}}\right)^2}, \qquad Nu = -\frac{k_{nf}H}{k_f(T_w - T_h)}\frac{\partial T}{\partial Z}\,|_{Z=h(t)}\,. \tag{3.32}$$

Consulting Equation (3.19), we obtain

$$\frac{H^2}{R^2}ReC_{fr} = \frac{1}{(1-\phi)^{2.5}\left((1-\phi) + \phi\frac{\rho_s}{\rho_f}\right)}f''(1), \qquad \sqrt{1-ct}Nu = -\frac{k_{nf}}{k_f}\theta'(1), \tag{3.33}$$

with local squeezed Reynolds number Re_L

$$Re_L = \frac{\rho_f \; RcH\sqrt{1-ct}}{\mu_f} \; . \tag{3.34}$$

3.2 Results and discussion

Results are illustrated for axial velocity $f(\eta)$, radial velocity $f'(\eta)$, temperature profile $\theta(\eta)$ and concentration field $h(\eta)$ to discuss the heat transport and behavior of fluid flow for flow parameters at definite values. Flow parameters are squeezing parameter Sq, the suction parameter s, Hartmann number Ha, the volume fraction coefficient ϕ, the Schmidt number Sc, the homogeneous reaction parameter k_1, the heterogeneous parameter k_2, and the thermal relaxation parameter γ. We fixed certain values for above flow parameters such that $s = 0.4$, $Sc = 1.0$, $\gamma = 0.5$, $Ha = 0.5$, $k_1 = 0.7$, $k_2 = 0.7$, $Pr = 6.2$, $\phi = 0.1$, $Sq = 1.0$ until they are specified. For both SWCNTs and MWCNTs, graphs are drawn. Figure 3.2 is sketched to portray the infuence of s suction parameter on axial velocity $f(\eta)$. Graph depicts that with the large values of parameter s, axial velocity increases. This is due to velocity profile accelerates for high suction, which results in opposite flow. In contrast with the lower plate, the effect of opposite flow is more dominant nearby the upper plate. To create an opposite flow close to the lower plate, presure gradient is the main reason. Due to this, large number of fluid particles move aside from the lower disk. Figure 3.3 illustrates that how positive and negative values of squeezed number Sq affect the radial velocity $f'(\eta)$. Graph depicts that for both SWCNTs and MWCNTs, velocity $f'(\eta)$ increases for contraction of disks *i.e.*, negative values, while for positive values when upper and lower plates are driving afar from each other, an opposite bahavior can be observed. In case of contraction ($Sq = -1, -2, -3.$) when both plates move towards each other, a squeezed force is experienced by the fluid which causes motion of the fluid with more velocity. Hence, velocity augments. Whereas for $Sq = 1, 2, 3..$ when both plates move far from each other, a gap is produced between the plates. The fluid moves in inverse direction to fill this gap and thus velocity reduces. For both SWC-

NTs and MWCNTs, impact of suction parameter is portrayed in Figures 3.4 and 3.5. It is examined in figure 3.4 that for escalating values of suction parameter s, radial velocity drops for MWCNTs. It is observed that velocity declines whenever suction influence is strengthened. Figure 3.5 exhibits the same results for SWCNTs. Figure 3.6 indicates the impact of volume fraction of nanoparticles ϕ for both SWCNTs and MWCNTs. It is observed in Figure 3.6 that for growing values of ϕ, velocity reduces close to the lower disk while augments after a certain distance towards the upper disk. However, in case of squeezing flow it is examined in Figure 3.7 that the temperature profile θ declines for cumulative values of volume fraction ϕ. Physically, thermal conductivity of nanofluid enhances using low concentration of nanoparticles. Hence, high nanoparticles concentration leads to decrease in temperature. In Figure 3.8, effect of Sq squeezed number is exhibited. In case of contraction of disks ($Sq = -1, -2, -3$), temperature profile $\theta(\eta)$ establishes diminishing behavior while escalating behavior when the disks are driving afar from each other *i.e.*, $Sq = 1, 2, 3$. The effect of relaxation parameter γ versus temperature $\theta(\eta)$ is deliberated in Figure 3.9. Higher values of γ leads to the augmentation in temperature profile $\theta(\eta)$ for both SWCNTs and MWCNTs. Figures $3.10 - 3.12$ are plotted for both SWCNTs and MWCNTs to discuss concentration field $h(\eta)$ versus k_1, k_2 and Sc. Figure 3.10 indicates that $h(\eta)$ decreases with the higher values of homogeneous reaction parameter k_1. The same outcome can be observed in figures 3.11 for k_2 heterogeneous reaction parameter. This is because concentration declines eventually when reactants are consumed throughout HH reactions. In Figure 3.12, the effect of Schmidt number is represented. Concentration profile is being reduced for increasing values of Schmidt number. As Sc is the ratio of momentum to mass diffusivity, greater Sc indicates the smaller mass diffusivity which results in the reduction in fluid concentration $h(\eta)$. For various values of squeezing parameter Sq, suction parameter s and thermal relaxation parameter γ, SFC and Nul are presented in Tables 3.2 and 3.3. SFC decreases for higher values of Sq and s whereas Nul increases for higher values of Sq, s and γ. For both SWCNTs and MWCNTs, Table 3.4 is presented for surface concentration $h(0)$ which

reduces with the increment in $k_1$and k_2.

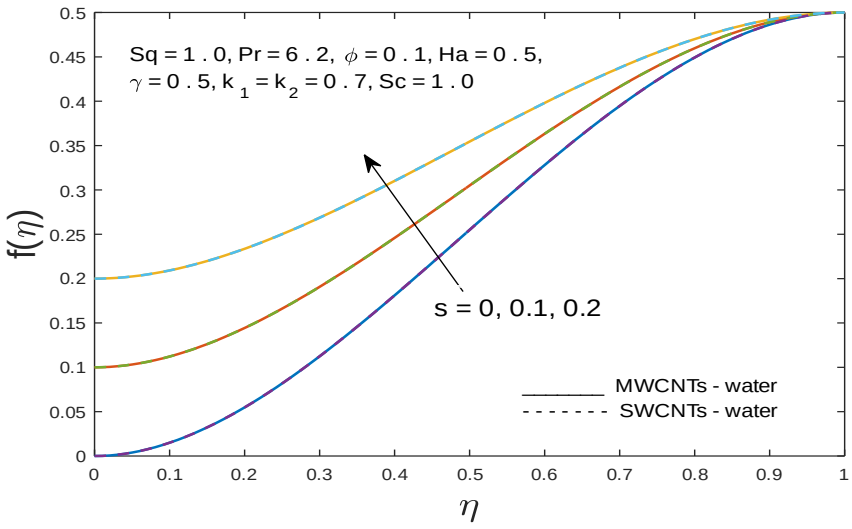

Fig. 3.2 Impact of s on axial velocity $f\,(\eta)$

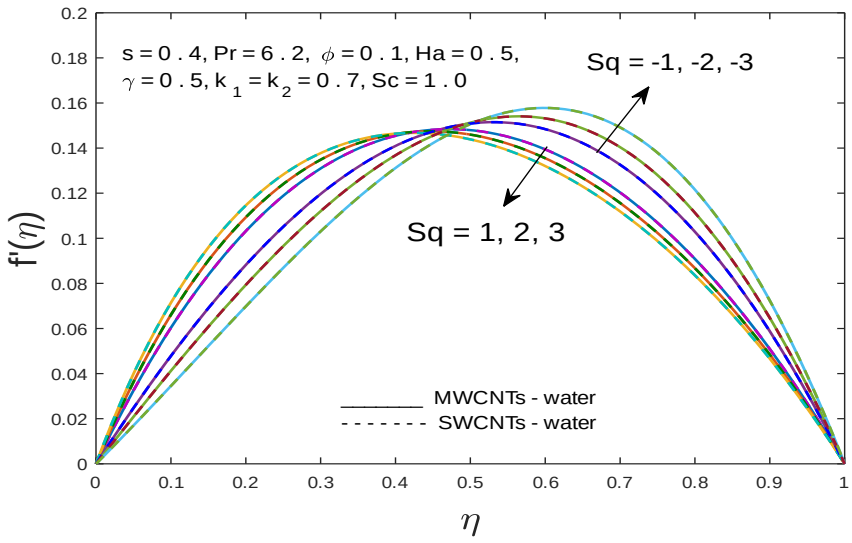

Fig. 3.3 Impact of Sq on radial velocity $f'\,(\eta)$

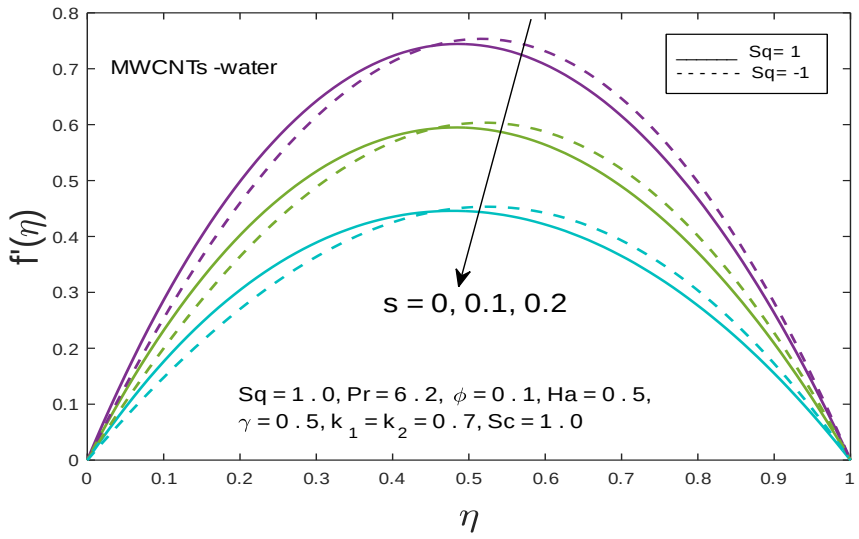

Fig. 3.4 Impact of s on radial velocity $f'(\eta)$ for MWCNTs

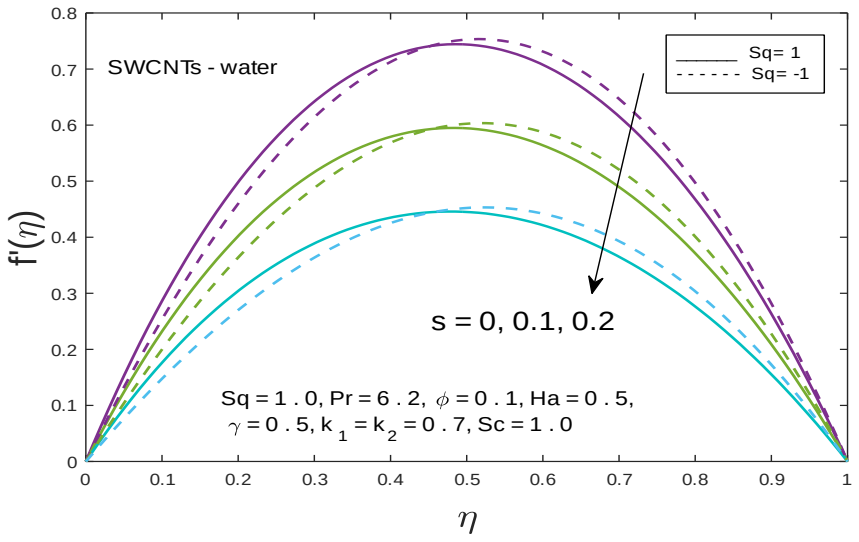

Fig. 3.5 Impact of s on radial velocity $f'(\eta)$ for SWCNTs

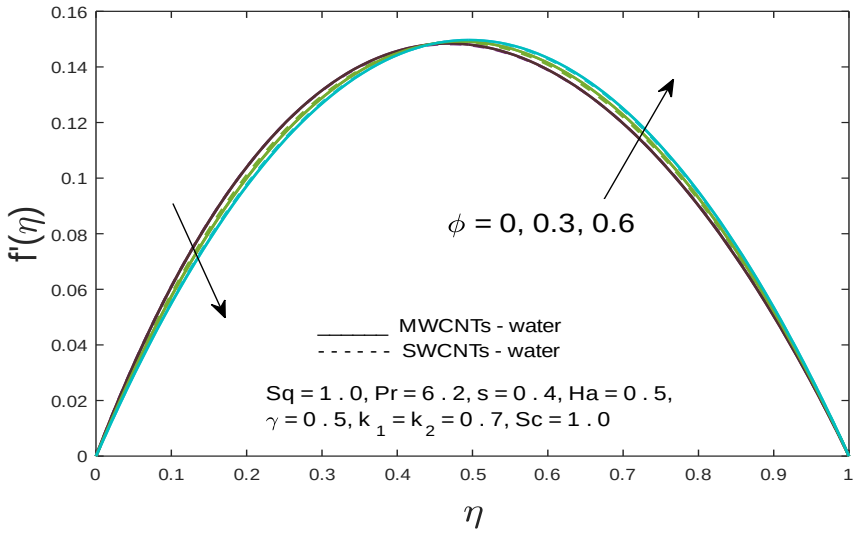

Fig. 3.6 Impact of ϕ on radial velocity $f'(\eta)$

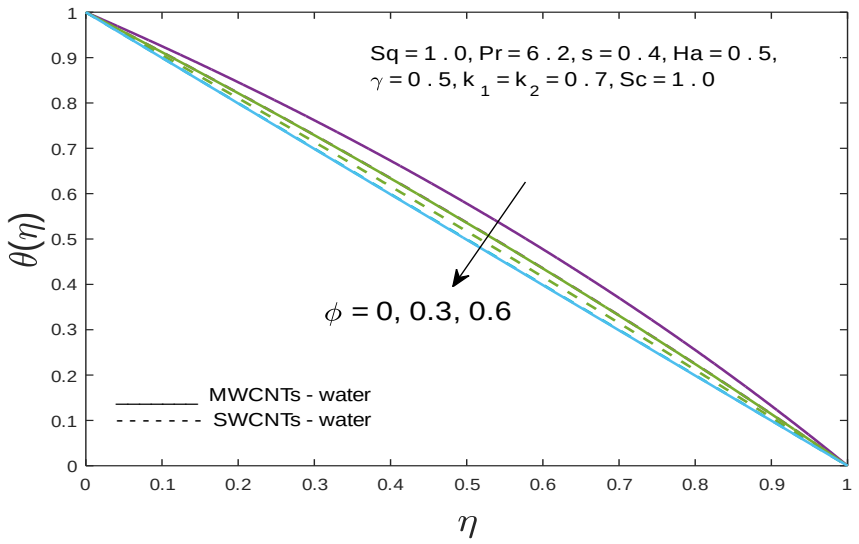

Fig. 3.7 Impact of ϕ on temperature distribution $\theta(\eta)$

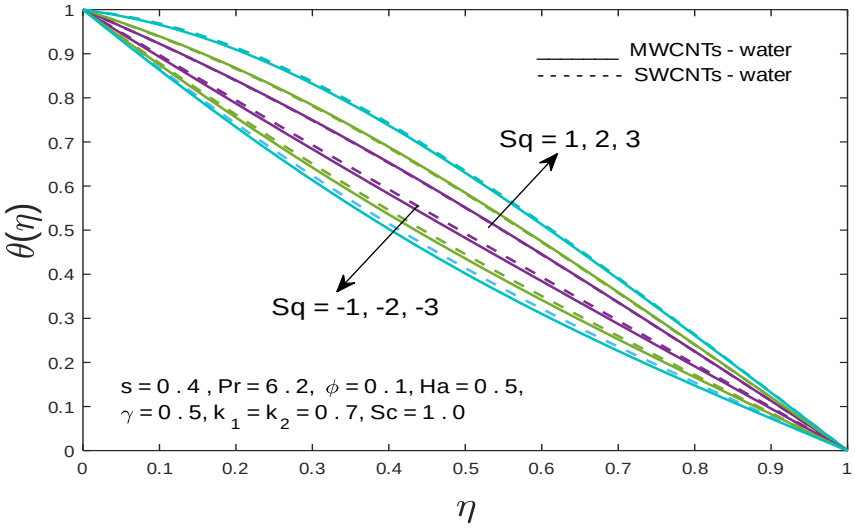

Fig. 3.8 Impact of Sq on temperature distribution $\theta(\eta)$

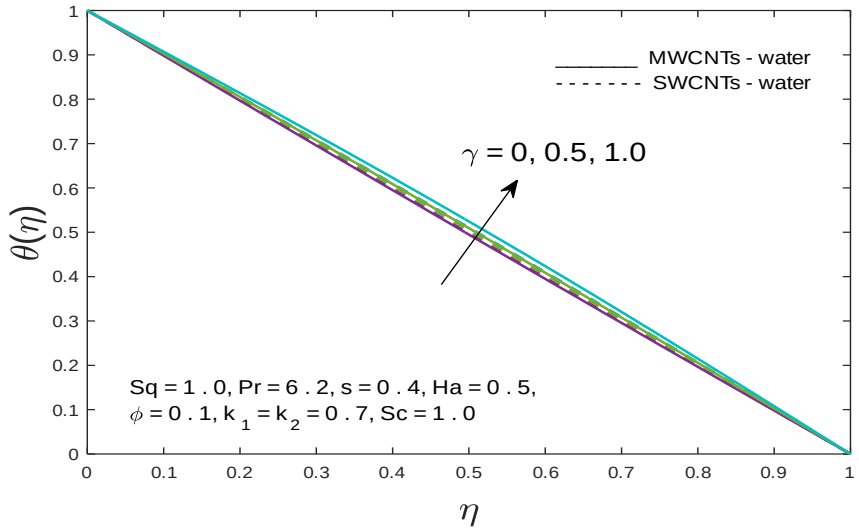

Fig. 3.9 Impact of γ on temperature distribution $\theta(\eta)$

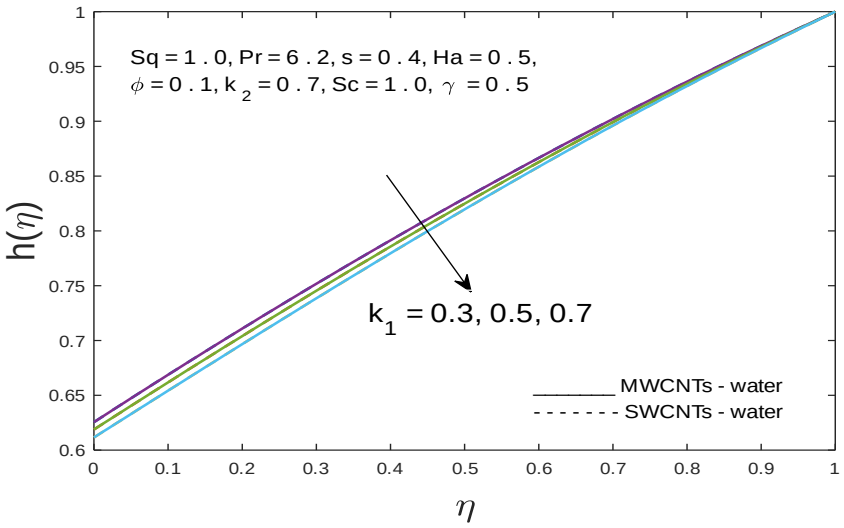

Fig. 3.10 Impact of k_1 on concentration profile $h(\eta)$

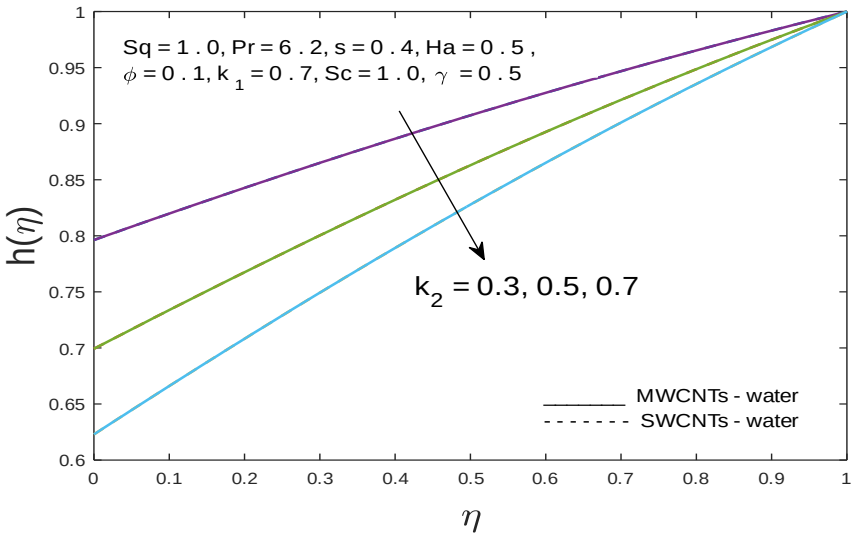

Fig. 3.11 Impact of k_2 on concentration profile $h(\eta)$

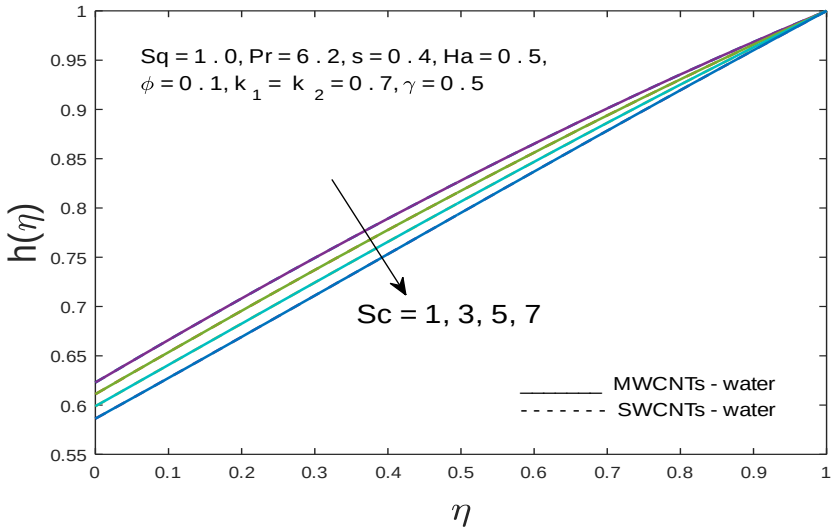

Fig. 3.12 Impact of Sc on concentration profile $h\,(\eta)$

Table 3.2 Impact of Squeezing Sq and suction parameters s on SFC $\left(\frac{H^2}{R^2}\right)\mathrm{Re}_r\, C_{fr}$ when $Sc = 1.0$, $\gamma = 0.5$, $Ha = 0.5$, $k_1 = 0.7$, $k_2 = 0.7$, $Pr = 6.2$, $\phi = 0.1$.

s	Sq	SFC for SWCNTs	SFC for MWCNTs
0.0	1.0	0.13983393	0.14835160
0.1		0.10895464	0.11565795
0.2		0.07947330	0.08441676
0.1	-1.0	0.01746634	0.01819335
	0.0	0.01051051	0.01150452
	1.0	0.01032101	0.01131235

Table 3.3 Impact of Squeezing Sq, suction parameters s and thermal relaxation parameter γ on Nul $(1-ct)^{\frac{1}{2}}\, Nu$ when $Sc = 1.0$, $Ha = 0.5$, $k_1 = 0.7$, $k_2 = 0.7$, $Pr = 6.2$,

$\phi = 0.1$.

Sq	s	γ	Nul for SWCNTs	Nul for MWCNTs
-1	0.4	0.5	1.343625	6.09528877
0			1.345840	6.11745513
1			1.348025	6.13941320
1	0		1.346456	6.12363146
	0.1		1.346843	6.12752401
	0.2		1.347234	6.13145122
		0	1.348025	6.13941320
		0.3	1.348027	6.13943734
		0.5	1.348031	6.13947355

Table 3.4 Impact of homogeneous k_1 and heterogeneous k_2 reaction coefficients on surface concentration $h(0)$ when $Sc = 1.0$, $Ha = 0.5$, $Sq = 0.5$, $s = 0.4$, $Pr = 6.2$, $\phi = 0.1$

k_1	k_2	$h(0)$ for SWCNTs	$h(0)$ for MWCNTs
0.3	0.7	0.25258956	0.25244606
0.5		0.12087726	0.12087205
0.7		0.04014484	0.04015474
0.7	0.3	0.05365630	0.05367049
	0.5	0.04909591	0.04592125
	0.7	0.04014484	0.04015474

Chapter 4

Radiative Darcy-Forchheimer squeezing carbon Nano-tubes suspended Nano-fluid flow between parallel disks

In this chapter, time-dependent magnetohydrodynamics (MHD) flow of squeezing nano-fluid water-based single-walled (SW) and multi-walled (MW) carbon nano-tubes (CNTs) amidst two parallel disks with the effects of homogeneous-heterogeneous reactions in a Darcy-Forchheimer penetrable media is discussed. The impacts of non-linear thermal radiation and melting heat tranfer are also deliberated. The requisite boundary layer equations are transformed into non-linear ordinary differential equations after consulting suitable similarity transformation. The acquired system of equations is addressed by bvp4c built in fuction of MATLAB scheme. The outcomes of the prominent parameters are portrayed for temperature, concentration fields, axial and radial velocities. It is perceived that temperature decreases as radiation parameter increases for both SWCNTs and MWCNTs.

4.1 Mathematical formulation

Consider an incompressible, unsteady 2D MHD flow of nano-fluid containing carbon nano-tubes with Darcy-Forchheimer permeable medium amidst two-infinite parallel disks by the length $Z = h(t) = H(1 - ct)^{0.5}$ with magnetic field strength $\frac{B_0}{\sqrt{1-ct}}$ normal to the disks. Two types of carbon nano-tubes, single-walled CNTs and multi-walled CNTs along with the base fluid (water) are considered. Let T_h be the temperature at upper disk $Z = h\,(t)$ and temperature T_m be the temperature of surface (lower plate) $Z = 0$. Moreover, the upper disk $Z = h(t)$ is moving to and fro with the velocity $\frac{dZ}{dt}$ from the fixed and porous lower disk $Z = 0$ (Figure-4.1). We have considered the cylindrical coordinate system (R, α, Z) and the velocity component V vanishes identically due to rotational flow symmetry $\left(\frac{\partial}{\partial \alpha} = 0\right)$. The direction of flow is vertically upward towards the $Z - axis$.

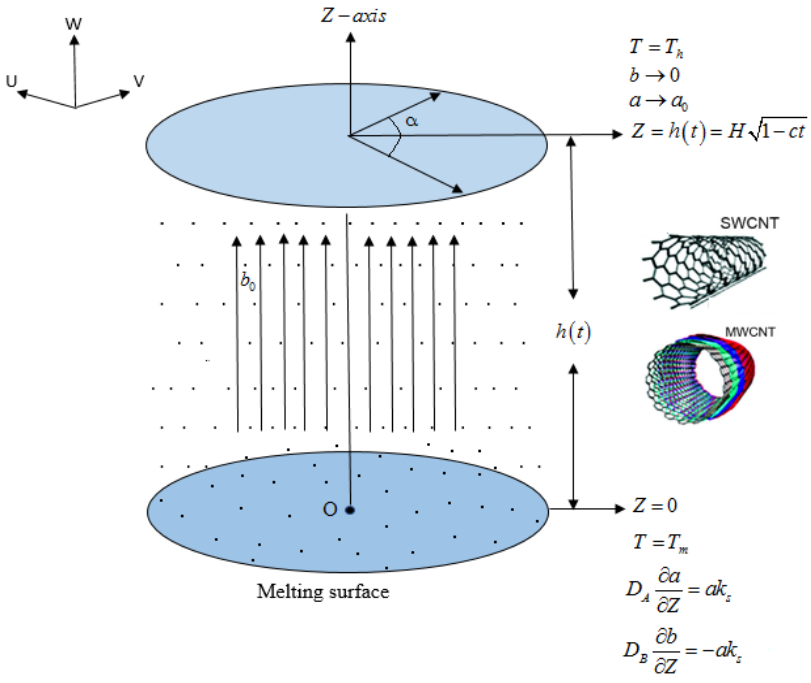

Fig. 4.1 Fluid geometry

By considering small Reynolds number, the induced magnetic field is not taken into consideration. We asssume a model, designed by Chaudhary and Merkin [44] for homo-geneous and hetero-geneous chemical reactions defined as:

$$A^* + 2B^* \rightarrow 3B^*, \qquad rate = k_c ab^2, \tag{4.1}$$

$$A^* \rightarrow B^*, \qquad \text{rate} = k_s a \ . \tag{4.2}$$

Here, A^* and B^* are chemical species. Concentrations for these chemical species are expressed by a, b and k_j, with $(j = c, s)$ where a, b and k_j are rate quantities. These reactions are presumed to be an isothermic. The equations of conservation of mass, momentum, energy and concentration are as follows:

$$\boldsymbol{\nabla}.\mathbf{V} = \mathbf{0}, \tag{4.3}$$

$$\rho_{nf}\frac{\mathbf{dV}}{\mathbf{dt}} = -\boldsymbol{\nabla}\mathbf{P} + \mu_{nf}\boldsymbol{\nabla}^2\mathbf{V} + \rho_{nf}\left[\sigma\left(\mathbf{J}\times\mathbf{B}\right) - \frac{\nu_{nf}\mathbf{V}}{K} - F^*\mathbf{V}^2\right], \tag{4.4}$$

$$\mathbf{T}_t + \mathbf{V}.\boldsymbol{\nabla}\mathbf{T} + \boldsymbol{\epsilon}\left[\mathbf{T}_{tt} + 2\mathbf{V}.\boldsymbol{\nabla}\mathbf{T}_t + \mathbf{V}_t.\nabla\mathbf{T} + \mathbf{V}.\boldsymbol{\nabla}\left(\mathbf{V}.\boldsymbol{\nabla}\mathbf{T}\right)\right]$$

$$= \frac{k_{nf}}{\left(\rho C_p\right)_{nf}}\boldsymbol{\nabla}.\left(\boldsymbol{\nabla}\mathbf{T}\right) - \boldsymbol{\nabla}.\mathbf{q}_r, \tag{4.5}$$

$$\frac{\mathbf{d}a}{\mathbf{dt}} = D_A\left(\boldsymbol{\nabla}^2 a\right) - k_c ab^2, \tag{4.6}$$

$$\frac{\mathbf{d}b}{\mathbf{dt}} = D_B\left(\boldsymbol{\nabla}^2 b\right) + k_c ab^2. \tag{4.7}$$

The governing equations from Equations $(4.3) - (4.7)$ are represented as:

$$\frac{\partial U}{\partial R} + \frac{U}{R} + \frac{\partial W}{\partial Z} = 0, \tag{4.8}$$

$$\frac{\partial U}{\partial t} + U\frac{\partial U}{\partial R} + W\frac{\partial U}{\partial Z} = -\frac{1}{\rho_{nf}}\frac{\partial P}{\partial R} + \frac{\mu_{nf}}{\rho_{nf}}\left(\frac{\partial^2 U}{\partial R^2} + \frac{1}{R}\frac{\partial U}{\partial R} - \frac{U}{R^2} + \frac{\partial^2 U}{\partial Z^2}\right)$$

$$-\sigma B^2(t)U - \frac{\nu_{nf}U}{K} - F^*U^2, \tag{4.9}$$

$$\frac{\partial W}{\partial t}+U\frac{\partial W}{\partial R}+W\frac{\partial W}{\partial Z}=-\frac{1}{\rho_{nf}}\frac{\partial P}{\partial Z}+\frac{\mu_{nf}}{\rho_{nf}}\left(\frac{\partial^2 W}{\partial R^2}+\frac{1}{R}\frac{\partial W}{\partial R}+\frac{\partial^2 W}{\partial Z^2}\right)$$
$$-\frac{\nu_{nf}W}{K}-F^{*}W^2, \tag{4.10}$$

$$\frac{\partial T}{\partial t}+U\frac{\partial T}{\partial R}+W\frac{\partial T}{\partial Z}+\varepsilon\begin{pmatrix}\frac{\partial^2 T}{\partial t^2}+\frac{\partial U}{\partial t}\frac{\partial T}{\partial R}+2U\frac{\partial^2 T}{\partial t\partial R}+2W\frac{\partial^2 T}{\partial t\partial Z}\\ +\frac{\partial W}{\partial t}\frac{\partial T}{\partial Z}+U\frac{\partial U}{\partial R}\frac{\partial T}{\partial R}+W\frac{\partial W}{\partial Z}\frac{\partial T}{\partial Z}+U\frac{\partial W}{\partial R}\frac{\partial T}{\partial Z}\\ +W\frac{\partial U}{\partial Z}\frac{\partial T}{\partial R}+2UW\frac{\partial^2 T}{\partial R\partial Z}+U^2\frac{\partial^2 T}{\partial R^2}+W^2\frac{\partial^2 T}{\partial Z^2}\end{pmatrix}$$
$$=\frac{k_{nf}}{(\rho C_p)_{nf}}(\frac{\partial^2 T}{\partial R^2}+\frac{1}{R}\frac{\partial T}{\partial R}+\frac{\partial^2 T}{\partial Z^2})-\frac{1}{(\rho C_p)_{nf}}\frac{\partial}{\partial Z}\left(q_{rd}\right), \tag{4.11}$$

$$\frac{\partial a}{\partial t}+U\frac{\partial a}{\partial R}+W\frac{\partial a}{\partial Z}=D_A\left(\frac{\partial^2 a}{\partial R^2}+\frac{1}{R}\frac{\partial a}{\partial R}+\frac{\partial^2 a}{\partial Z^2}\right)-k_c ab^2, \tag{4.12}$$

$$\frac{\partial b}{\partial t}+U\frac{\partial b}{\partial R}+W\frac{\partial b}{\partial Z}=D_B\left(\frac{\partial^2 b}{\partial R^2}+\frac{1}{R}\frac{\partial b}{\partial R}+\frac{\partial^2 b}{\partial Z^2}\right)+k_c ab^2. \tag{4.13}$$

Here, D_A and D_B are the diffusion coefficients. The suitable boundary conditions are described by

$$\begin{aligned}U &= 0, \qquad k_{nf}\left(\frac{\partial T}{\partial Z}\right)_{Z=0}=\rho_{nf}\left[C_s\left(T_m-T_0\right)+L\right]W\left(R,0\right), \\ T &= T_m, \qquad D_A\frac{\partial a}{\partial Z}=k_s a, \qquad D_B\frac{\partial b}{\partial Z}=-k_s a, \qquad \text{at} \;\; Z=0,\end{aligned} \tag{4.14}$$

$$U=0, \quad W=\frac{dh}{dt}, \quad T=T_h, \quad a\rightarrow a_{0,} \;\; b\rightarrow 0, \qquad \text{at} \;\; Z=h(t). \tag{4.15}$$

Mathematically, thermophysical properties are:

$$\mu_{nf}=\frac{\mu_f}{(1-\phi)^{2.5}}, \quad \nu_{nf}=\frac{\mu_{nf}}{\rho_{nf}}, \quad \rho_{nf}=(1-\phi)\,\rho_f+\phi\rho_{CNT}\,,$$

$$(\rho C_p)_{nf}=(1-\phi)\,(\rho C_p)_f+\phi\,(\rho C_p)_{CNT}\;\;,$$

$$\frac{k_{nf}}{k_f}=\frac{(1-\phi)+2\phi\frac{k_{CNT}}{k_{CNT}-k_f}\ln\frac{k_{CNT}+k_f}{2k_f}}{(1-\phi)+2\phi\frac{k_{CNT}}{k_{CNT}-k_f}\ln\frac{k_{CNT}+k_f}{2k_f}}. \tag{4.16}$$

From Equation (4.11), by utilizing Roseland thermal radiation approximation [46] we get

the value of q_{rd} as:

$$q_{rd} = -\frac{4\sigma^*}{3k^*}\frac{\partial T^4}{\partial Z}. \tag{4.17}$$

4.1.1 Similarity transformations

Similarity transformations are defined as:

$$U = \frac{cR}{2(1-ct)}f'(\eta), \qquad W = -\frac{cH}{\sqrt{(1-ct)}}f(\eta), \qquad \eta = \frac{Z}{H\sqrt{1-ct}},$$

$$B(t) = \frac{B_0}{\sqrt{1-ct}}, \qquad h(\eta) = \frac{a}{a_0}, \qquad g(\eta) = \frac{b}{a_0}, \qquad \theta(\eta) = \frac{T-T_m}{T_h-T_m}. \tag{4.18}$$

Using above transformations, incompressibility condition is satisfied and Equations (4.9)−(4.13) are transformed into the followings:

$$\frac{1}{(1-\phi)^{2.5}}\left[f''''(\eta) - \lambda Ref''(\eta)\right] - Sq\left[(1-\phi) + \phi\frac{\rho_c}{\rho_f}\right]$$

$$\begin{bmatrix} 3f''(\eta) + \eta f'''(\eta) \\ -2f(\eta) f'''(\eta) + ReF f'(\eta) f''(\eta) \end{bmatrix} - Ha^2 f''(\eta) = 0, \tag{4.19}$$

$$\frac{k_{nf}}{k_f}\left[\left(1 + R_d\left(1 + (\theta_w - 1)\theta(\eta)\right)^3\right)\theta'(\eta)\right]' + SqPr\left[(1-\phi) + \phi\frac{(\rho C_p)_s}{(\rho C_p)_f}\right]$$

$$\begin{bmatrix} 2f(\eta)\theta'(\eta) - \eta\theta'(\eta) - \\ \gamma\left(\begin{array}{c} \eta^2\theta''(\eta) - 4\eta f(\eta)\theta''(\eta) - 2\eta f'(\eta)\theta'(\eta) + 4f(\eta) f'(\eta)\theta'(\eta) \\ +4f^2(\eta)\theta''(\eta) + 3\eta\theta'(\eta) - 6f(\eta)\theta'(\eta) \end{array}\right) \end{bmatrix} = 0, \tag{4.20}$$

$$\frac{1}{Sc}h''(\eta) - \frac{\eta}{2}h'(\eta) + f(\eta)h'(\eta) - k_1 h(\eta) g^2(\eta) = 0, \tag{4.21}$$

$$\frac{\delta}{Sc}g''(\eta) - \frac{\eta}{2}g'(\eta) + f(\eta)g'(\eta) + k_1 h(\eta) g^2(\eta) = 0, \tag{4.22}$$

with boundary conditions

$$f'(0)=0, \qquad \theta(0)=0, \qquad \frac{k_{nf}}{k_f}Me\ \theta'(0)+\epsilon_0 PrRef(0)=0,$$

$$h'(0)=k_2 h(0), \qquad \delta g'(0)=-k_2 h(0), \qquad \text{at} \quad \eta=0, \tag{4.23}$$

$$f(1)=\frac{1}{2}, \qquad f'(1)=0, \qquad \theta(1)=1, \qquad g(1)\to 0,$$

$$h(1)\to 1, \qquad \text{at} \quad \eta=1. \tag{4.24}$$

with

$$\delta=\frac{D_B}{D_A}. \tag{4.25}$$

From Equations (4.1) and (4.2), chemical species A^* and B^* cannot be analogous, but both can be identical in volume. However, presuming that diffusion species D_B and D_A are identical ($\delta=1$), we have

$$h(\eta)+g(\eta)=1. \tag{4.26}$$

Now by applying the above property, Equations (4.21) and (4.22) take the form

$$\frac{1}{Sc}h''(\eta)-\frac{\eta}{2}h'(\eta)+f(\eta)h'(\eta)-k_1 h(\eta)(1-h(\eta))^2=0, \tag{4.27}$$

with boundary conditions

$$h'(0)=k_2 h(0), \qquad \text{at} \quad \eta=0,$$

$$h(1)\to 1, \qquad \text{at} \quad \eta=1, \tag{4.28}$$

where dimensionless parameters are:

$$Sq=\frac{cH^2}{2\nu_f}, \qquad Ha=\left(\frac{\sigma_f B_0^2 H^2}{\mu_f}\right)^{\frac{1}{2}}, \qquad Pr=\frac{\mu_f C_p}{k_f}, \qquad Sc=\frac{cH^2}{D_A},$$

$$Re = \frac{cH^2}{\nu_f}, \qquad F = F^* R = \frac{C_b}{\sqrt{K}} R, \qquad \lambda = \frac{\nu_f}{Kc}, \qquad R_d = \frac{16\sigma^* T_m^3}{3k_{nf}k^*},$$

$$Me = \frac{C_f\left(T_h - T_m\right)}{L + C_s\left(T_m - T_0\right)}, \qquad \gamma = \frac{\epsilon c}{2\left(1 - ct\right)}, \qquad k_1 = \frac{k_c a_0^2 \left(1 - ct\right)}{c},$$

$$k_2 = \frac{k_s}{D_A} H\left(1 - ct\right)^{\frac{1}{2}}, \qquad \epsilon_0 = \left((1 - \phi) + \phi \frac{\rho_s}{\rho_f}\right), \qquad \theta_w = \frac{T_h}{T_m}. \tag{4.29}$$

SFC and local Nul is classified by:

$$C_{fr} = \frac{\mu_{nf}\left(\frac{\partial U}{\partial Z} + \frac{\partial W}{\partial R}\right)_{Z=h(t)}}{\frac{1}{2}\rho_{nf}\left(-\frac{cH}{2(1-ct)^{\frac{1}{2}}}\right)^2}, \qquad Nu = \frac{k_{nf} H}{k_f\left(T_h - T_m\right)}\left[\left(q_r\right)_w - \left(\frac{\partial T}{\partial Z}\right)_{Z=h(t)}\right]. \tag{4.30}$$

Using Equation (4.18), we obtain

$$\frac{H^2}{R^2} Re_r C_{fr} = \frac{1}{\left(1 - \phi\right)^{2.5}\left((1 - \phi) + \phi \frac{\rho_s}{\rho_f}\right)} f''\left(1\right),$$

$$\sqrt{1 - ct} Nu = -\left(\frac{k_{nf}}{k_f} + R_d\left(1 + \left(\theta_w - 1\right)\theta\left(1\right)\right)^3\right)\theta'\left(1\right), \tag{4.31}$$

with squeezed Reynolds number Re_L

$$Re_L = \frac{\rho_f \; RcH\sqrt{1 - ct}}{\mu_f}. \tag{4.32}$$

4.2 Results and discussion

In this section, the outcomes are depicted for temperature $\theta\left(\eta\right)$ and concentration profiles $h\left(\eta\right)$, axial $f\left(\eta\right)$ and radial velocity $f'\left(\eta\right)$ to discuss the heat transport and behavior of fluid flow for flow parameters at distinct values. Impacts of appropriate parameters $i.e.$, Hartmann number Ha, squeezing parameter Sq, the volume fraction coefficient ϕ, the Schmidt number Sc, the homogeneous-heterogeneous parameters k_1 and k_2, the thermal relaxation parameter γ, Prandtl number Pr, local inertia coefficient F, porosity parameter λ, radiation parameter R_d, Reynolds number Re, temperature ratio coefficient θ_w,

melting heat transit coefficient Me are examined diagrammatically. For both SWCNTs and MWCNTs, consequences are drawn. In Figures 4.2, 4.3(a) and 4.3(b) the velocity and dimensionless temperature are examined for Hartmann number Ha. The retarding impact of Hartmann number Ha on radial velocity $f'(\eta)$ can be observed in Figure 4.2 when disks are driving afar from each other. At the middle of disks, velocity is greater in case of $Ha = 0$. But, with increase in magnetic field, velocity decreases. This is since the magnetic field generates a Lorentz force which resists the movement of fluid flow. Hence, velocity decreases at the middle of the disks. In Figures 4.3(a) and 4.3(b) the dimensionless temperature is examined for Hartmann number Ha. The dimensionless temperature augments for higher values of Hartmann number Ha. Physically, strength of magnetic field increases due to increment in Ha which provides more heat in the fluid, hence, temperature increases. Figure 4.4 illustrates that how positive and negative values of squeezed number Sq affect the velocity $f'(\eta)$. Graph depicts that for both single and multi-walled CNTs, velocity profile increases for contraction of disks $i.e.$, negative values of Sq, whereas for positive values when upper and lower plates are driving afar from each other, an opposite behavior can be observed. In case of contraction ($Sq = -1, -2, -3, ...$) a squeezed force is experienced by the fluid which causes motion of the fluid with more velocity. Hence, velocity augments. Whereas for $Sq = 1, 2, 3, ...$ when both disks move far from each other, a gap is produced between the disks. The fluid moves in inverse direction to fill this gap; thus, velocity reduces in radial direction. In Figure 4.5 effect of squeezed number Sq is exhibited versus temperature profile. In case of contraction of disks ($Sq = -1, -2, ...$), temperature profile establishes diminishing behavior whereas opposite trend is seen when the disks are driving afar from each other ($i.e., Sq = 1, 2, ..$). An inverse impact of melting heat transfer parameter Me can be observed in Figures 4.6 and 4.7 for velocity $f'(\eta)$ and temperature $\theta(\eta)$ profiles. Due to melting heat transmit parameter Me molecular motion enhances from hot fluid toward cold fluid surface which causes augmentation in velocity. In contrast with temperature field, as the convective flow causes heat transfer to the melting surface more promptly which causes the decrease

in temperature $\theta(\eta)$. Figures 4.8 and 4.9 depicts the effect of local inertia coefficient F on velocity $f'(\eta)$ and temperature $\theta(\eta)$ of fluid flow. It can be observed that local inertia coefficient F has an inverse influence on both fields. Here, velocity $f'(\eta)$ falls whereas temperature $\theta(\eta)$ augments. As porous media causes resistance in a fluid flow which results in the reduction in dimensionless velocity. In case of temperature field $\theta(\eta)$, a resistive force provides more energy to the fluid. Due to this, temperature $\theta(\eta)$ enhances. To perceive the impacts of Reynolds number Re on both fields, Figures 4.10 (a), 4.10(b) and 4.11 are illustrated. For higher values of Re, temperature $\theta(\eta)$ and radial velocity $f'(\eta)$ falls whereas axial velocity $f(\eta)$ increases. The increment in Re increases the axial velocity and reduces the radial velocity because when upper disk moves (towards $Z-axis$) away from the lower plate, a gap is produced. To cover this free space, fluid motion increases towards $Z-axis$ (in axial direction) which leads to the increase in axial velocity whereas decrease in radial velocity. The effects of porosity parameter λ on radial velocity $f'(\eta)$ are drawn in Figure 4.12. Velocity $f'(\eta)$ falls for higher values of λ. Since, the porosity of porous media causes high resistivity to the fluid flow; hence, velocity $f'(\eta)$ declines. Figure 4.13 is drawn to observe the behavior of temperature ratio number θ_w on fluid temperature $\theta(\eta)$. A retarding effect of on dimensionless temperature can be seen. Physically, augmentation in θ_w $\left(\theta_w = \frac{T_h}{T_m}\right)$ causes decrease in temperature on melting surface. Du to this energy loss can be seen and hence temperature decreases. Figures 4.14 and 4.15 show the impacts of nano-particle volume fraction ϕ on radial velocity $f'(\eta)$ and temperature $\theta(\eta)$. Since, an augmentation of nano-particles within base fluid (water) leads to the higher thermal conductivity. Due to this, particles get close to each other which results in the velocity reduction (Figure 4.14). On the other side, in Figure 4.15 for ordinary fluid ($i.e.$, $\phi = 0$, in the absence of volume proportion) the temperature field is highest when the disks are driving afar from each other ($i.e.$, $Sq = 1$) while an augmentation of volume proportion causes reduction in temperature of the fluid. Figure 4.16 demonstrates the effects of R_d on temperature $\theta(\eta)$. The temperature decreases for larger values of R_d. Here, the radiation parameter R_d $\left(R_d = \frac{16\sigma^* T_m^3}{3k_{nf}k^*}\right)$ has

direct relation with the melting temperature T_m. Melting temperature is increased with the increment in R_d. As all energy from radiation is used in the melting process; thus, temperature decreases. Physically, high radiation parameter values provide more radiative heat energy into the system, causing augmentation in temperature. In Figure 4.17 the impacts of thermal relaxation coefficient γ are drawn. Higher values of γ leads to the augmentation in dimensionless temperature $\theta(\eta)$. Figures 4.18 and 4.19 are sketched to portray the effects of Pr on velocity $f'(\eta)$ and temperature $\theta(\eta)$ fields. Physically, an augmentation in Pr leads to the weaker thermal diffusivity which causes a retardation effect in temperature. Hence, velocity decreases. But the melting heat causes increase in temperature for higher values of Pr. Figures 4.20-4.23 are plotted for both SWCNTs and MWCNTs to deliberate the concentration field $h(\eta)$. Figure 4.20 indicates that $h(\eta)$ decreases with the higher values of k_1. The same outcome can be detected in Figure 4.21 for k_2. It is deduced that concentration profile reduces eventually throughout HH reactions as reactants are expended throughout both reactions. The effects of Sc are portrayed in Figure 4.22. Concentration profile $h(\eta)$ is being reduced for increasing values of Sc. Since, Sc is the ratio of momentum to mass diffusivity, greater indicates the smaller mass diffusivity which causes reduction in fluid concentration $h(\eta)$. Figure 4.23 depicts the influence of melting heat transit coefficient Me on concentration field $h(\eta)$. It can be seen that Me has a retarding impact on concentration profile $h(\eta)$. Influences of melting parameter Me and squeezing number Sq on Nul are depicted in Figure 4.24. It can be perceived that augmentation in Me and Sq causes an increment in Nul. Figure 4.25 is sketched to portray the impact of radiation coefficient R_d and temperature ratio coefficient θ_w on Nul. Nul falls for greater values of R_d and θ_w. From Figure 4.26, a retarding effect of porosity parameter λ against local inertia coefficient F can be seen for

SFC.

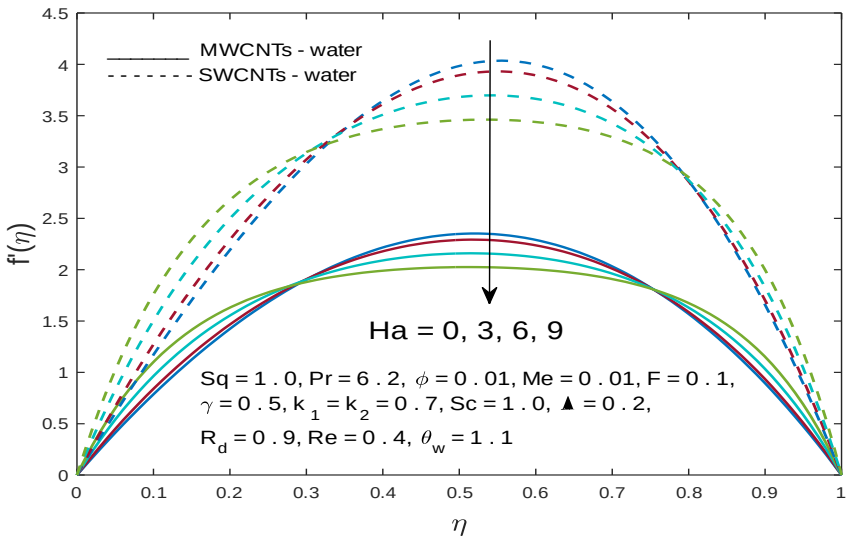

Fig. 4.2 Effect of Ha on radial velocity $f'(\eta)$

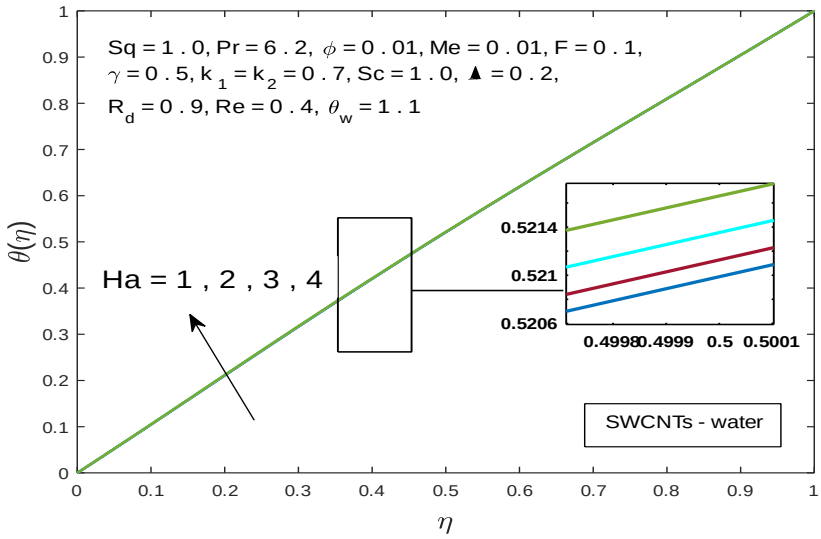

Fig. 4.3 (a) Effect of Ha on temperature distribution $\theta(\eta)$ for SWCNTs

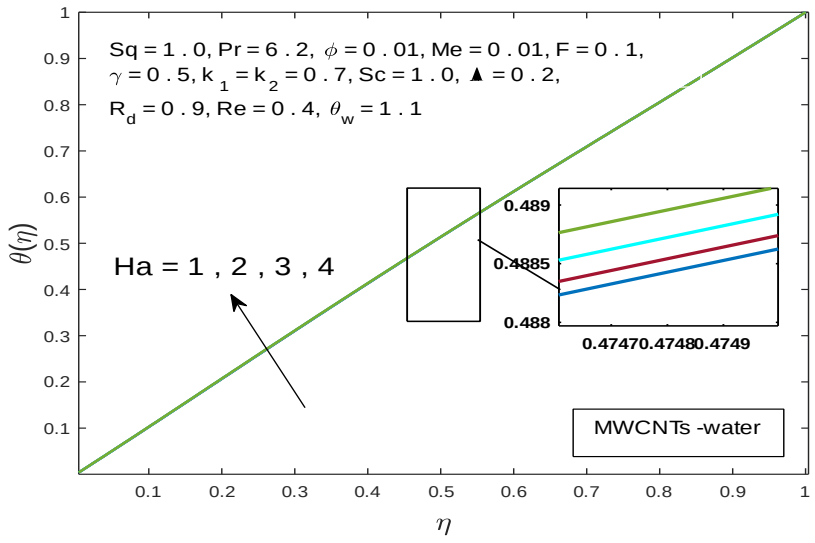

Fig. 4.3 (b) Effect of Ha on temperature distribution $\theta\,(\eta)$ for MWCNTs

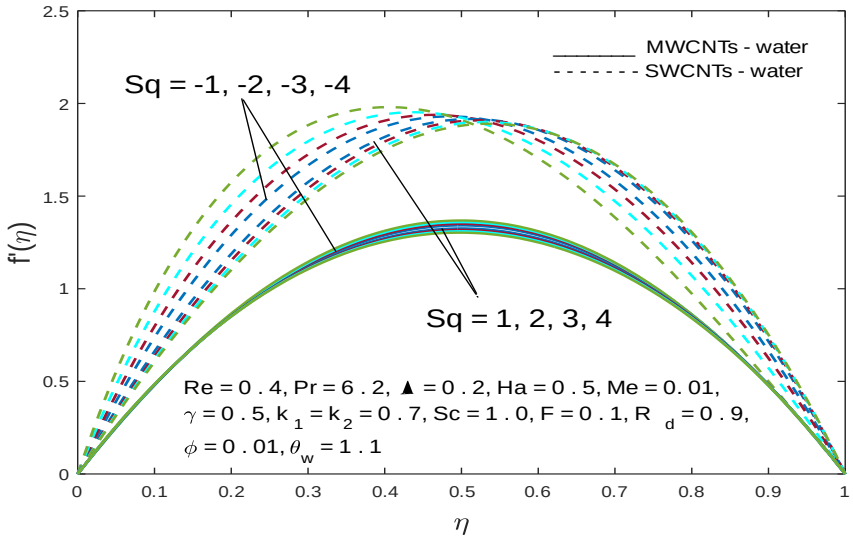

Fig. 4.4 Effect of Sq on radial velocity $f'\,(\eta)$

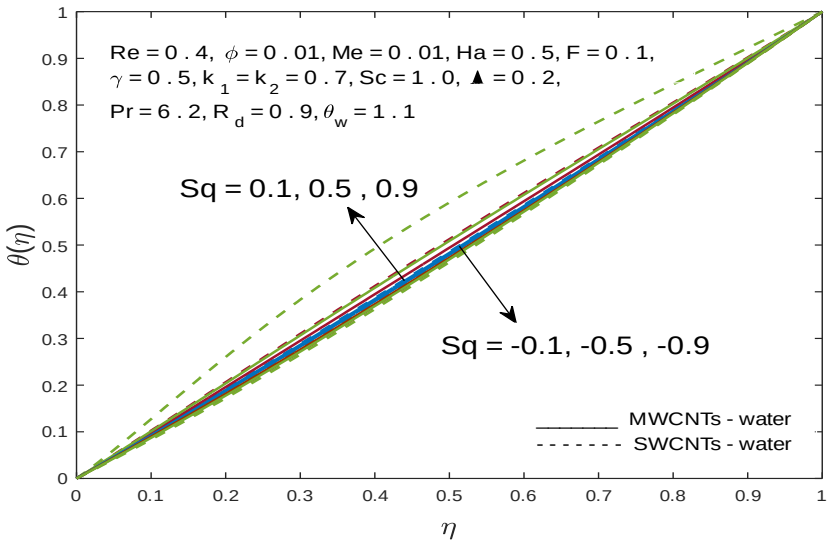

Fig. 4.5 Effect of Sq on temperature distribution $\theta(\eta)$

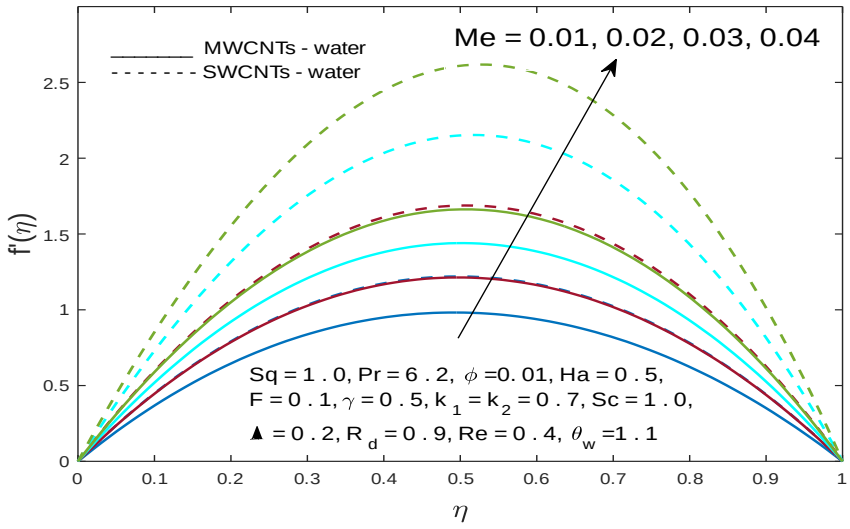

Fig. 4.6 Effect of Me on radial velocity $f'(\eta)$

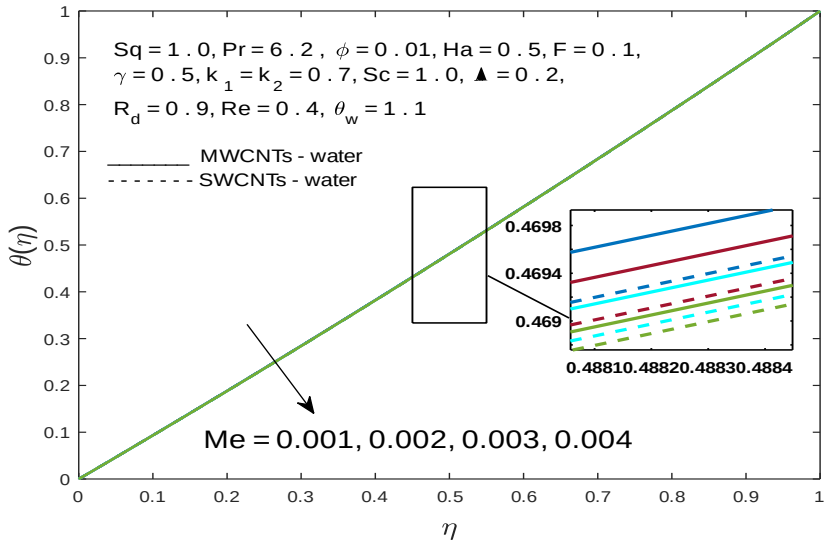

Fig. 4.7 Effect of Me on temperature distribution $\theta(\eta)$

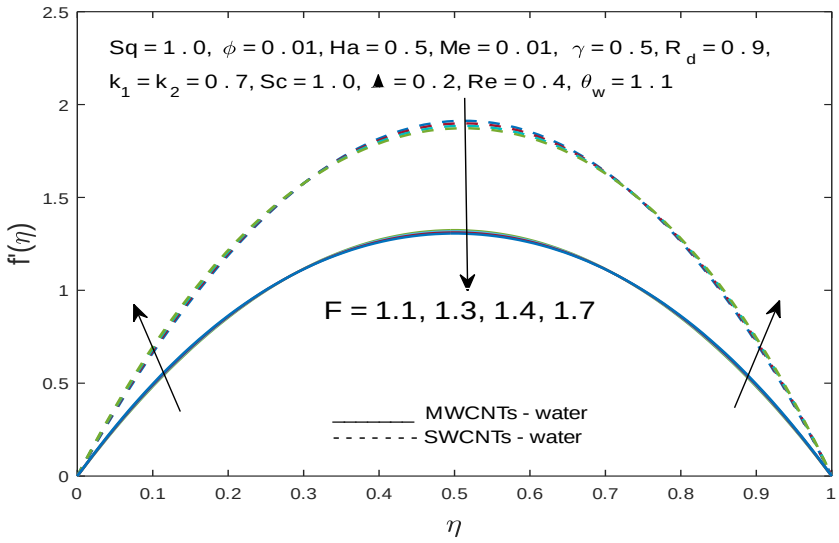

Fig. 4.8 Effect of F on radial velocity $f'(\eta)$

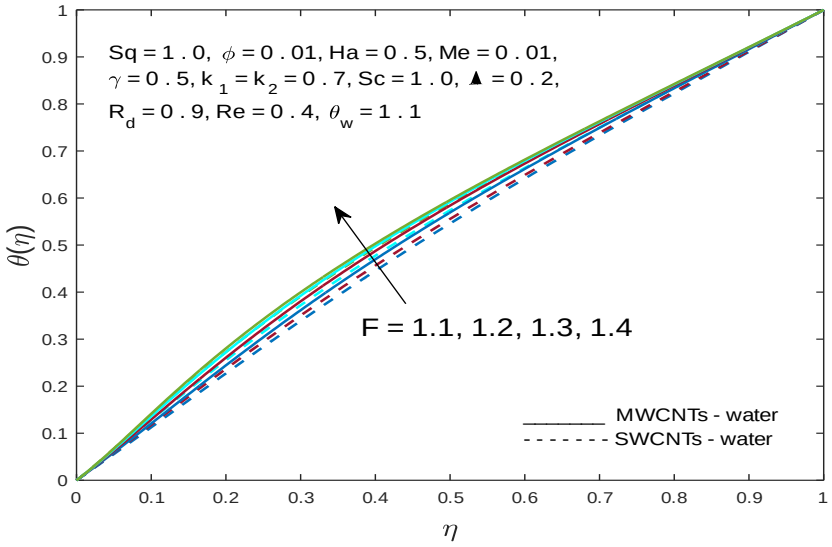

Fig. 4.9 Effect of F on temperature distribution $\theta(\eta)$

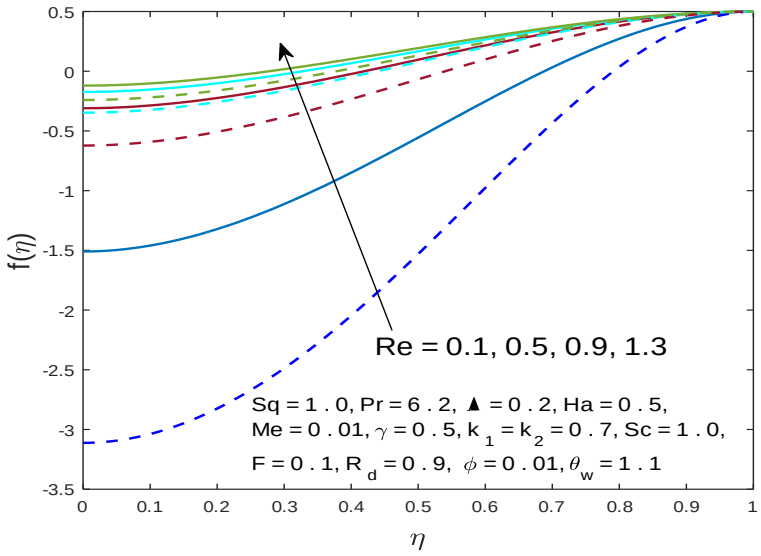

Fig. 4.10 (a) Effect of Re on axial velocity $f(\eta)$

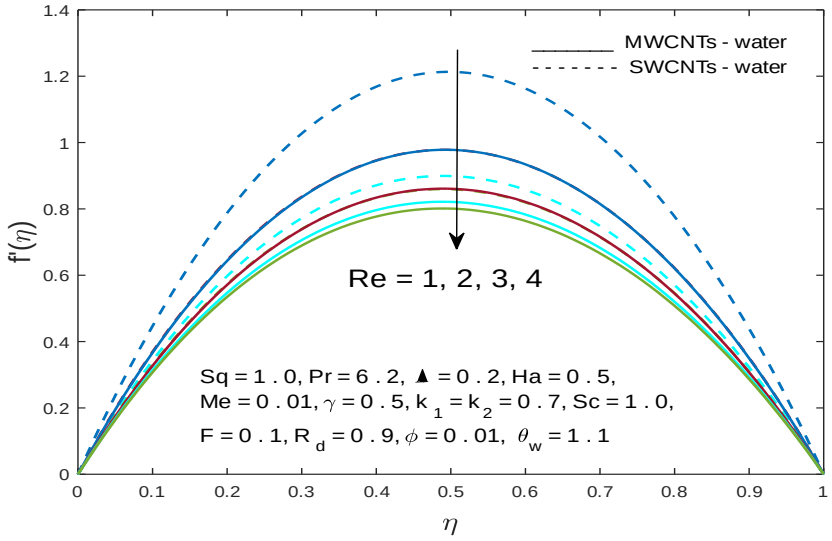

Fig. 4.10 (b) Effect of Re on radial velocity $f'(\eta)$

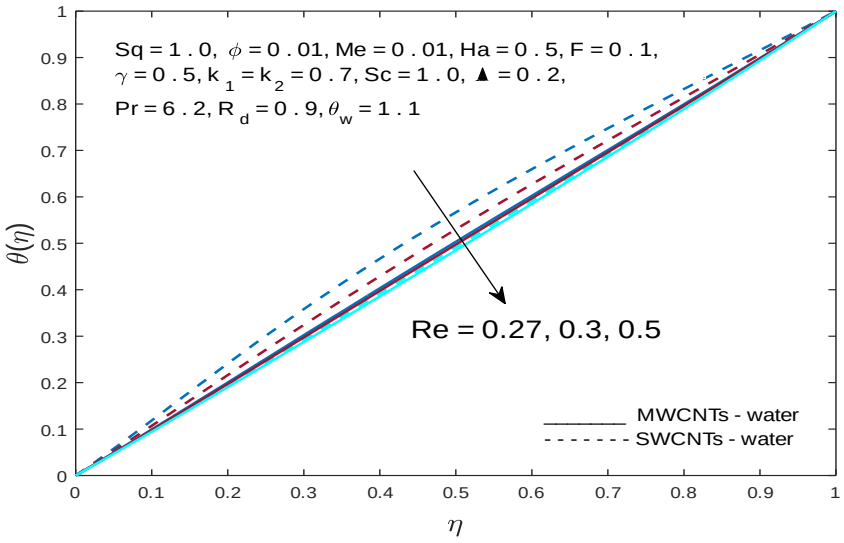

Fig. 4.11 Effect of Re on temperature distribution $\theta(\eta)$

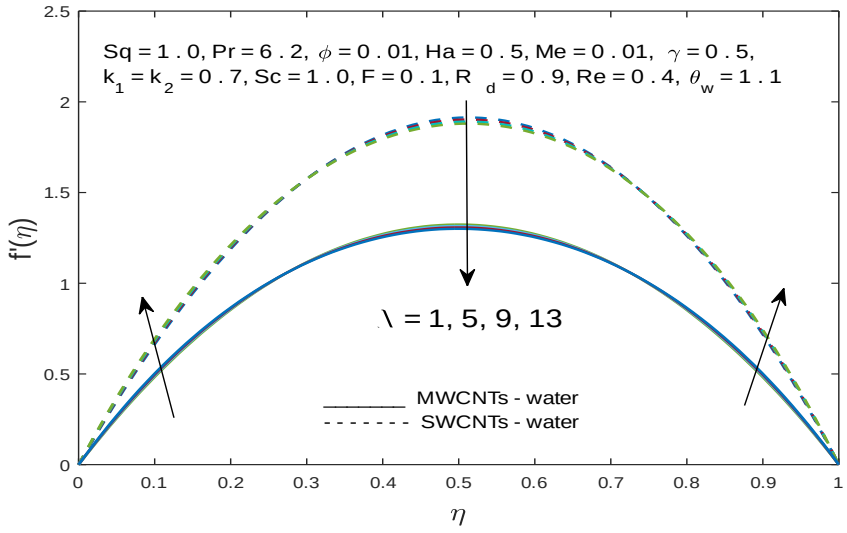

Fig. 4.12 Effect of λ on radial velocity $f'(\eta)$

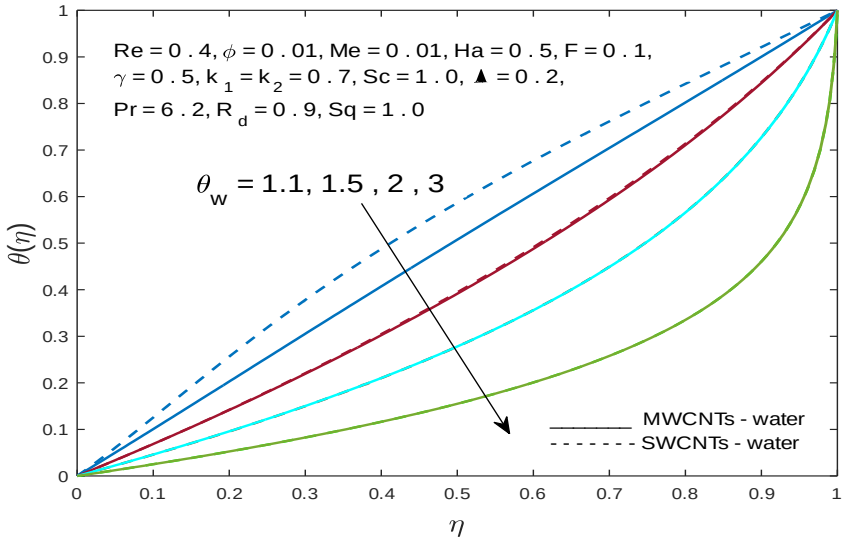

Fig. 4.13 Effect of θ_w on temperature distribution $\theta(\eta)$

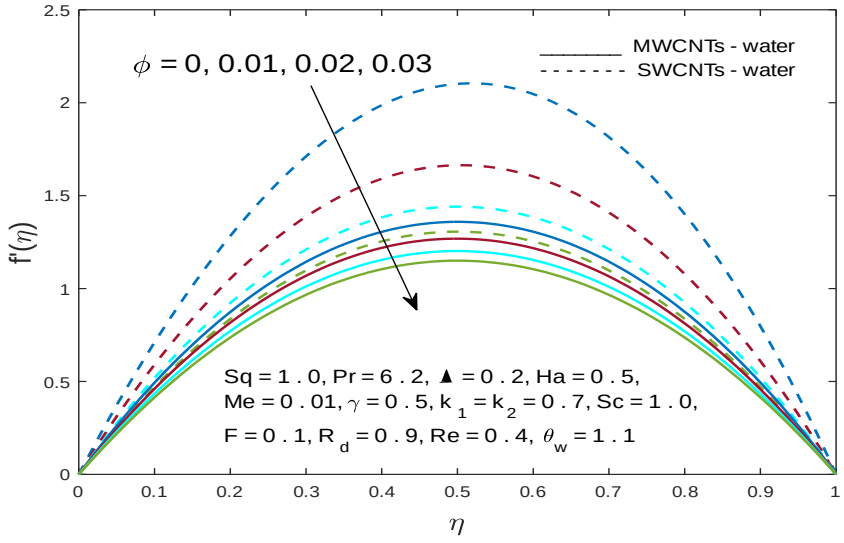

Fig. 4.14 Effect of ϕ on radial velocity $f'(\eta)$

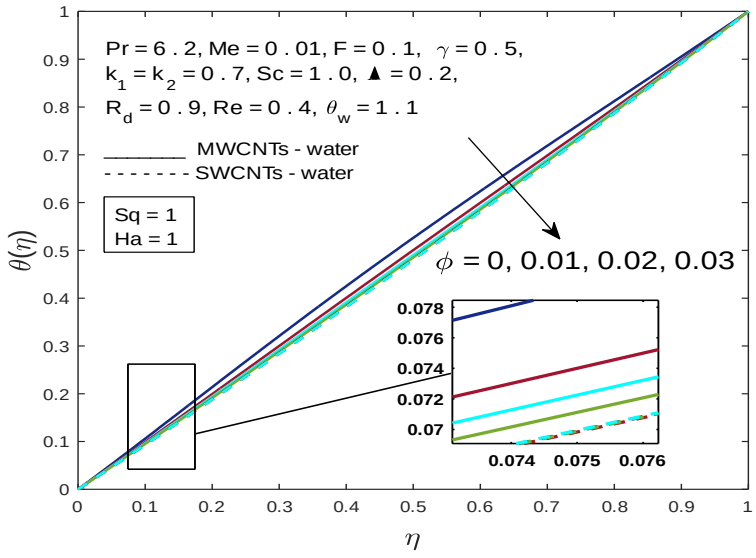

Fig. 4.15 Effect of ϕ on temperature distribution $\theta(\eta)$

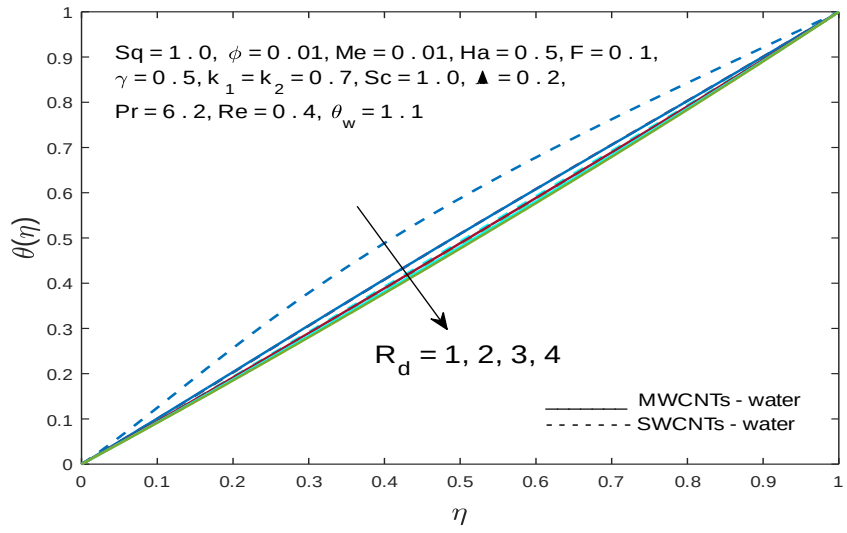

Fig. 4.16 Effect of R_d on temperature distribution $\theta(\eta)$

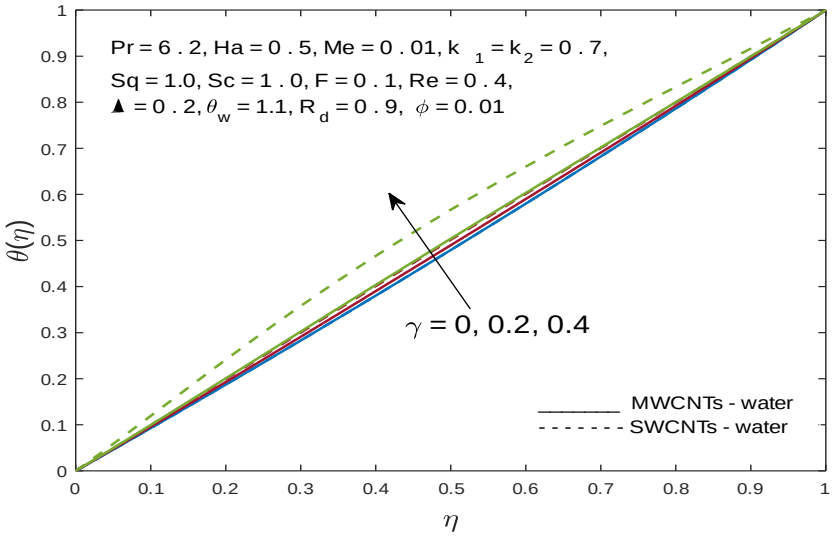

Fig. 4.17 Effect of γ on temperature distribution $\theta(\eta)$

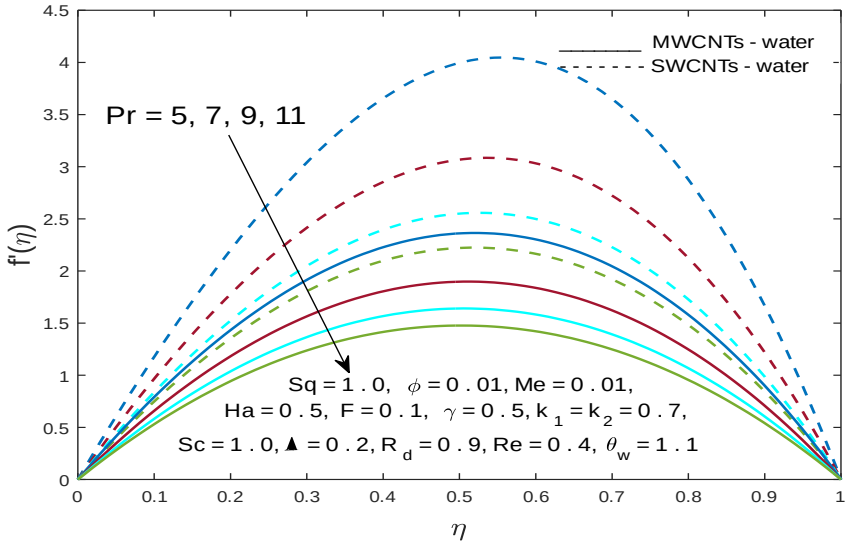

Fig. 4.18 Effect of Pr on radial velocity $f'(\eta)$

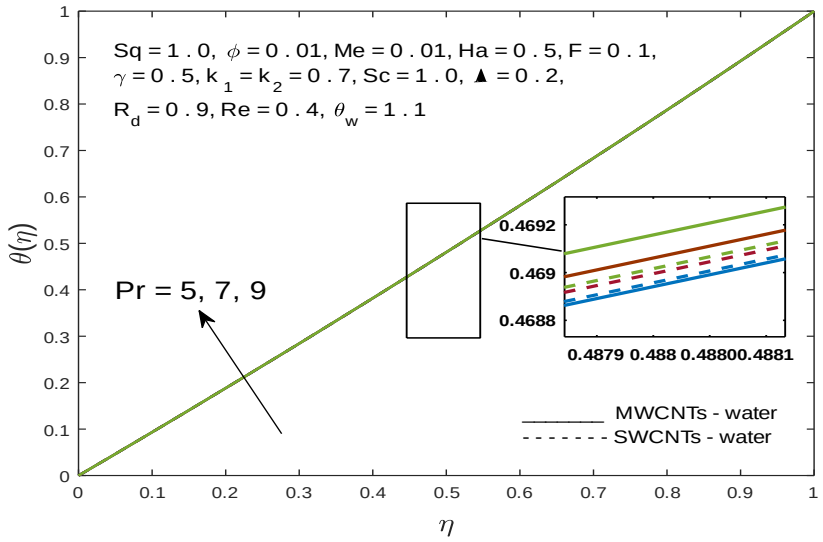

Fig. 4.19 Effect of Pr on temperature distribution $\theta(\eta)$

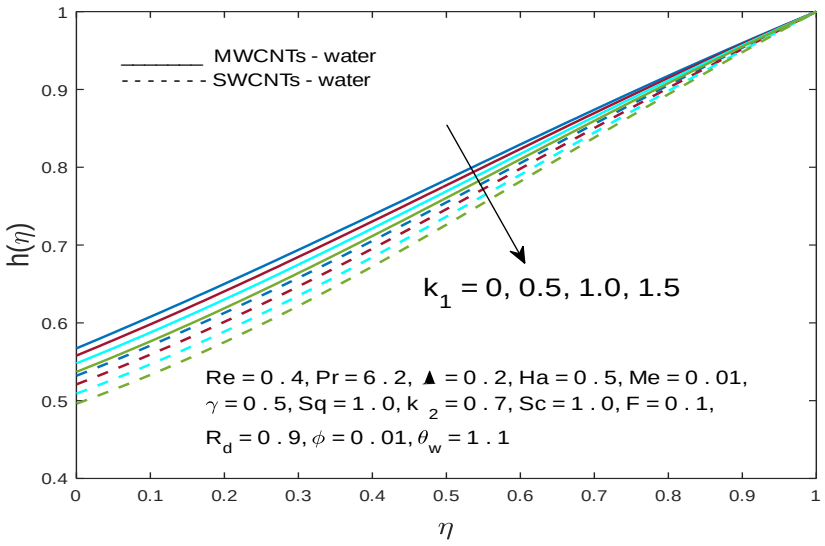

Fig. 4.20 Effect of k_1 on concentration profile $h(\eta)$

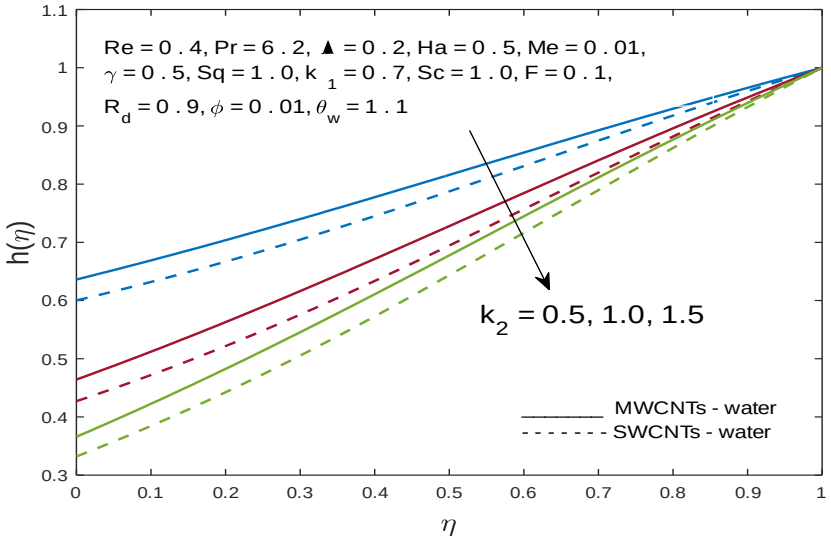

Fig. 4.21 Effect of k_2 on concentration profile $h(\eta)$

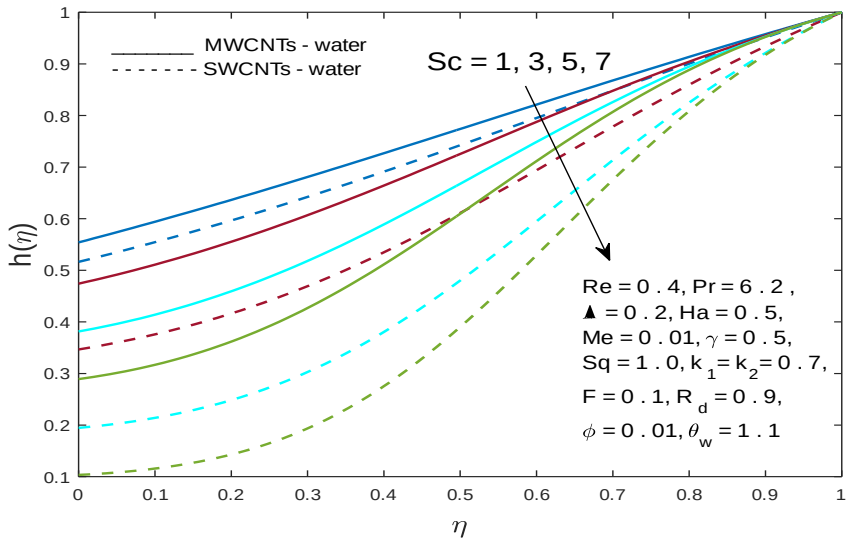

Fig. 4.22 Effect of Sc on concentration profile $h\,(\eta)$

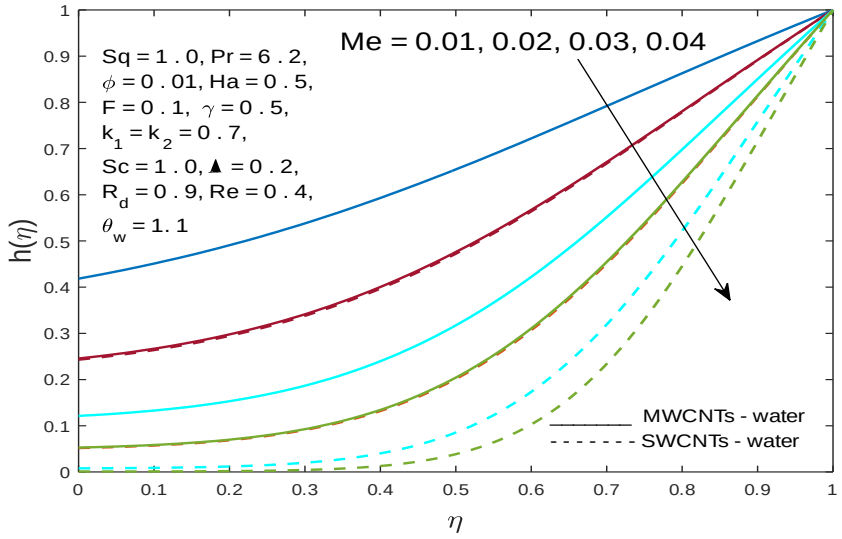

Fig. 4.23 Effect of Me on concentration profile $h\,(\eta)$

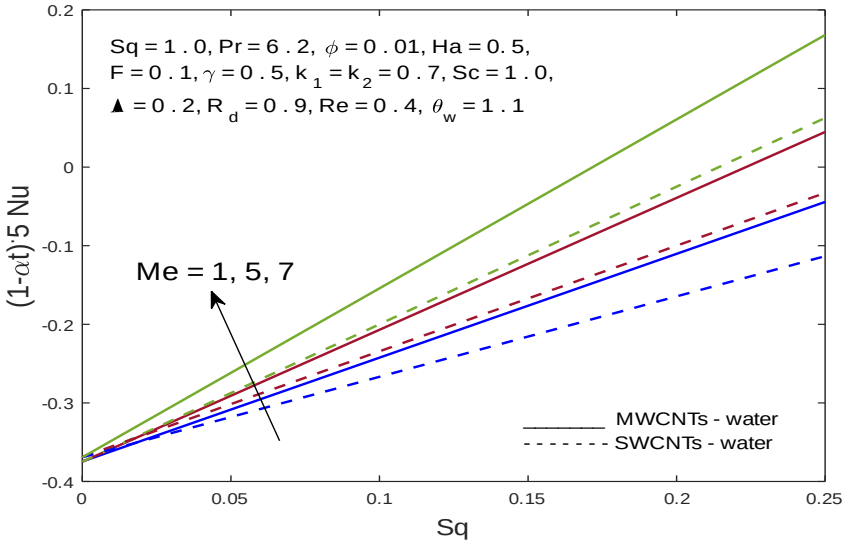

Fig. 4.24 Effect of Me and Sq on Nul

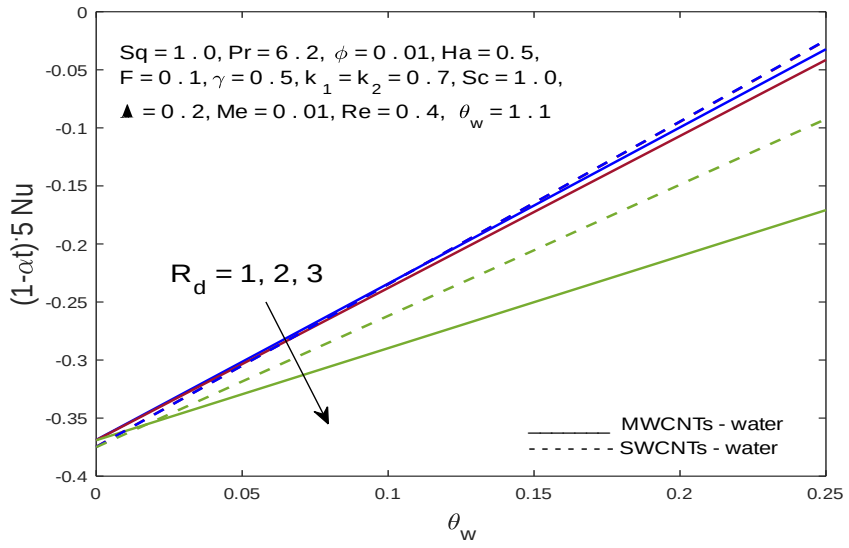

Fig. 4.25 Effect of R_d and θ_w on Nul

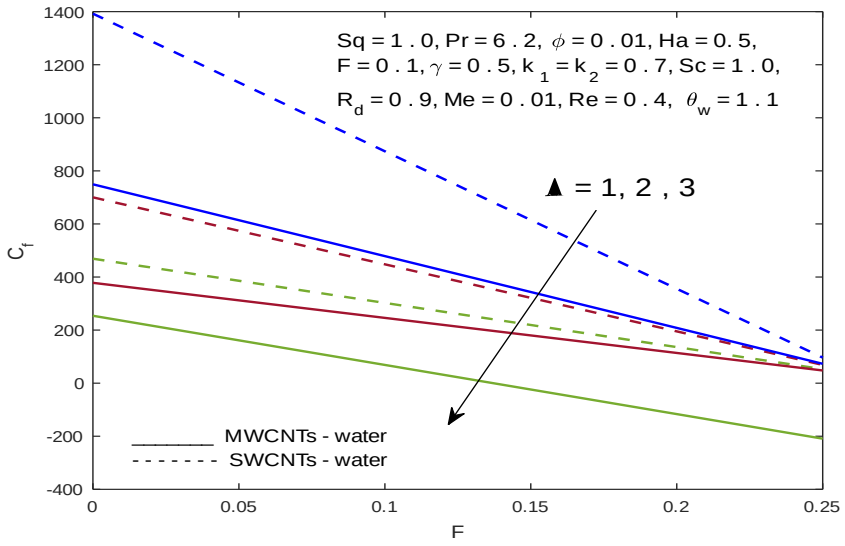

Fig. 4.26 Effect of λ and F on SFC

Chapter 5

Conclusions and future work

We studied two problems in this thesis. First one is review work while other is extended work. Conclusions for both problems are as follows:

5.1 Chapter 3

- For squeezing parameter Sq, Nusselt number increases while Skin friction shows an inverse effect for both cases ($i.e.$, single and multi-walled CNTs).
- The velocity distribution augments for increment in suction parameter s.
- For both single and multi-walled CNTs, homo-heterogeneous reactions coefficients k_1 and k_2 has a retarding impact on concentration field $h(\eta)$.
- The dimensionless temperature $\theta(\eta)$ increases for thermal relaxation parameter γ while exhibits an inverse effect for volume fraction parameter ϕ.

5.2 Chapter 4

- An augmentation in radiation parameter R_d exhibits reduction in dimensionless temperature $\theta(\eta)$.

- Local inertia coefficient F has an opposite impact on radial velocity $f'(\eta)$ and temperature field $\theta(\eta)$ (reduction in velocity while augmentation in temperature).
- Melting parameter has a retarding effect on temperature profile $\theta(\eta)$ while radial velocity $f'(\eta)$ increases due to melting.
- The concentration field $h(\eta)$ falls for an enhancing values of melting heat transfer parameter Me.
- The porosity coefficient λ has a retarding influence on radial velocity $f'(\eta)$.
- The fluid temperature $\theta(\eta)$ decays for growing values of temperature ratio coeffcient θ_w.
- Skin friction coefficient is reduced for large values of Porosity parameter λ against local inertia coefficient F and Local Nusselt number increases with the higher melting effects.

5.3 Future work

The present work may be extended to the followings:

- Any other non-Newtonian fluid along with appropriate boundary conditions.
- Bio-convective nano-fluid with microorganisms.
- Boundary conditions also be changed to second order slip.
- Flow over a curve surface with activation energy.

Bibliography

[1] Pierre Prevost (1832), Exposition e´le´mentaire des principes qui ser ent de base a la the´orie de la chaleur rayonnante, faisant suite a l'ou rage intitule´ du calorique rayonnant (Geneva and Paris: Abraham Cherbuliez,), p. 71. Prevost's theory was often referred to as the "theory of exchanges."

[2] Stefan, J. (1891). Über die Theorie der Eisbildung, insbesondere über die Eisbildung im Polarmeere. Annalen der Physik, 278(2), 269-286.

[3] Cattaneo, C. (1948). Sulla conduzione del calore. Atti Sem. Mat. Fis. Univ. Modena, 3, 83-101.

[4] Tibullo, V., & Zampoli, V. (2011). A uniqueness result for the Cattaneo–Christov heat conduction model applied to incompressible fluids. Mechanics Research Communications, 38(1), 77-79.

[5] Darcy, H. P. G. (1856). Les Fontaines publiques de la ville de Dijon. Exposition et application des principes à suivre et des formules à employer dans les questions de distribution d'eau, etc. V. Dalamont.

[6] Forchheimer, P. (1901). Wasserbewegung durch boden. Z. Ver. Deutsch, Ing., 45, 1782-1788.

[7] Muskat, M. (1938). The flow of homogeneous fluids through porous media. Soil Science, 46(2), 169.

[8] Das, S. K., Choi, S. U., & Patel, H. E. (2006). Heat transfer in nanofluids—a review. Heat Transfer Engineering, 27(10), 3-19.

[9] Yu, W., France, D. M., Choi, S. U., & Routbort, J. L. (2007). Review and assessment of nanofluid technology for transportation and other applications (No. ANL/ESD/07-9). Argonne National Lab.(ANL), Argonne, IL (United States).

[10] Uddin, M. & Al kalbani, Sami Khalaf Saif & Rahman, M. & Alam, Shariful & Al-Salti, Nasser & Eltayeb, Ibrahim. (2016). Fundamentals of Nanofluids: Evolution, Applications and New Theory. International Journal of Biomathematics and Systems Biology. 2. 1-32.

[11] Sheikholeslami, M., Ganji, D. D., & Ashorynejad, H. R. (2013). Investigation of squeezing unsteady nanofluid flow using ADM. Powder Technology, 239, 259-265.

[12] Mittal, R. C., & Pandit, S. (2017). Numerical simulation of unsteady squeezing nanofluid and heat flow between two parallel plates using wavelets. International Journal of Thermal Sciences, 118, 410-422.

[13] Ramzan, M., Sheikholeslami, M., Saeed, M., & Chung, J. D. (2019). On the convective heat and zero nanoparticle mass flux conditions in the flow of 3D MHD Couple Stress nanofluid over an exponentially stretched surface. Scientific Reports, 9(1), 1-13.

[14] Bilal, M., & Ramzan, M. (2019). Hall current effect on unsteady rotational flow of carbon nanotubes with dust particles and nonlinear thermal radiation in Darcy–Forchheimer porous media. Journal of Thermal Analysis and Calorimetry, 138(5), 3127-3137.

[15] Lu, D., Ramzan, M., Mohammad, M., Howari, F., & Chung, J. D. (2019). A thin film flow of nanofluid comprising carbon nanotubes influenced by Cattaneo-Christov heat flux and entropy generation. Coatings, 9(5), 296.

[16] Suleman, M., Ramzan, M., Ahmad, S., Lu, D., Muhammad, T., & Chung, J. D. (2019). A numerical simulation of Silver–Water nanofluid flow with impacts of Newtonian heating and homogeneous–heterogeneous reactions past a nonlinear stretched cylinder. Symmetry, 11(2), 295.

[17] Lu, D., Li, Z., Ramzan, M., Shafee, A., & Chung, J. D. (2019). Unsteady squeezing carbon nanotubes based nano-liquid flow with Cattaneo–Christov heat flux and homogeneous–heterogeneous reactions. Applied Nanoscience, 9(2), 169-178.

[18] Iijima, S. (1991). Helical microtubules of graphitic carbon. nature, 354(6348), 56-58.

[19] De Volder, M. F., Tawfick, S. H., Baughman, R. H., & Hart, A. J. (2013). Carbon nanotubes: present and future commercial applications. Science, 339(6119), 535-539.

[20] Hayat, T., Ayub, T., Muhammad, T., Alsaedi, A., & Mustafa, M. (2018). On Darcy-Forchheimer squeezed flow of carbon nanotubes between two parallel disks. International Journal of Numerical Methods for Heat & Fluid Flow.

[21] Stefan, M.J. (1874). Versuch uber die scheinbare adhesion, Akademie Der Wissenschaften in Wien. Mathematik-Naturwissen.

[22] Leider, P. J., & Bird, R. B. (1974). Squeezing flow between parallel disks. I. Theoretical analysis. Industrial & Engineering Chemistry Fundamentals, 13(4), 336-341.

[23] Qayyum, A., Awais, M., Alsaedi, A., & Hayat, T. (2012). Unsteady squeezing flow of Jeffery fluid between two parallel disks. Chinese Physics Letters, 29(3), 034701.

[24] Haq, R. U., Hammouch, Z., & Khan, W. A. (2016). Water-based squeezing flow in the presence of carbon nanotubes between two parallel disks. Thermal Science, 20(6), 1973-1981.

[25] Hayat, T., Haider, F., Muhammad, T., & Alsaedi, A. (2018). Darcy–Forchheimer squeezed flow of carbon nanotubes with thermal radiation. Journal of Physics and Chemistry of Solids, 120, 79-86.

[26] Hashmi, M. M., Hayat, T., & Alsaedi, A. (2012). On the analytic solutions for squeezing flow of nanofluid between parallel disks. Nonlinear Analysis: Modelling and Control, 17(4), 418-430.

[27] Mahmood, M., Asghar, S., & Hossain, M. A. (2007). Squeezed flow and heat transfer over a porous surface for viscous fluid. Heat and Mass Transfer, 44(2), 165-173.

[28] Hayat, T., Haider, F., Muhammad, T., & Alsaedi, A. (2018). Darcy–Forchheimer squeezed flow of carbon nanotubes with thermal radiation. Journal of Physics and Chemistry of Solids, 120, 79-86.

[29] Jha, B. K., & Kaurangini, M. L. (2011). Approximate analytical solutions for the nonlinear Brinkman-Forchheimer-extended Darcy flow model. Applied Mathematics, 2(12), 1432-1436.

[30] Nasir, S., Shah, Z., Islam, S., Khan, W., Bonyah, E., Ayaz, M., & Khan, A. (2019). Three dimensional Darcy-Forchheimer radiated flow of single and multiwall carbon nanotubes over a rotating stretchable disk with convective heat generation and absorption. AIP Advances, 9(3), 035031.

[31] Khan, M. I., Hayat, T., & Alsaedi, A. (2017). Numerical analysis for Darcy-Forchheimer flow in presence of homogeneous-heterogeneous reactions. Results in Physics, 7, 2644-2650.

[32] Hayat, T., Imtiaz, M., Alsaedi, A., & Kutbi, M. A. (2015). MHD three-dimensional flow of nanofluid with velocity slip and nonlinear thermal radiation. Journal of Magnetism and Magnetic Materials, 396, 31-37.

[33] S. Mukhopadhyay, S. (2013). Slip effects on MHD boundary layer flow over an exponentially stretching sheet with suction/blowing and thermal radiation. Ain Shams Engineering Journal, 4(3), 485-491.

[34] Sheikholeslami, M., Ganji, D. D., Javed, M. Y., & Ellahi, R. (2015). Effect of thermal radiation on magnetohydrodynamics nanofluid flow and heat transfer by means of two phase model. Journal of Magnetism and Magnetic Materials, 374, 36-43.

[35] Mohyud-Din, S. T., & Khan, S. I. (2016). Nonlinear radiation effects on squeezing flow of a Casson fluid between parallel disks. Aerospace Science and Technology, 48, 186-192.

[36] Epstein, M., & Cho, D. H. (1976). Melting heat transfer in steady laminar flow over a flat plate. Journal of Heat Transfer, 98(3).

[37] Hayat, T., Hussain, Z., Alsaedi, A., & Ahmad, B. (2016). Heterogeneous-homogeneous reactions and melting heat transfer effects in flow with carbon nanotubes. Journal of Molecular Liquids, 220, 200-207.

[38] Krishnamurthy, M. R., Prasannakumara, B. C., Gireesha, B. J., & Gorla, R. S. R. (2016). Effect of chemical reaction on MHD boundary layer flow and melting heat transfer of Williamson nanofluid in porous medium. Engineering Science and Technology, an International Journal, 19(1), 53-61.

[39] Christov, C. I. (2009). On frame indifferent formulation of the Maxwell–Cattaneo model of finite-speed heat conduction. Mechanics Research Communications, 36(4), 481-486.

[40] Han, S., Zheng, L., Li, C., & Zhang, X. (2014). Coupled flow and heat transfer in viscoelastic fluid with Cattaneo–Christov heat flux model. Applied Mathematics Letters, 38, 87-93.

[41] Lu, D., Ramzan, M., Mohammad, M., Howari, F., & Chung, J. D. (2019). A thin film flow of nanofluid comprising carbon nanotubes influenced by Cattaneo-Christov heat flux and entropy generation. Coatings, 9(5), 296.

[42] Ramzan, M., Bilal, M., & Chung, J. D. (2016). Effects of MHD homogeneous-heterogeneous reactions on third grade fluid flow with Cattaneo-Christov heat flux. Journal of Molecular Liquids, 223, 1284-1290.

[43] Lu, D., Li, Z., Ramzan, M., Shafee, A., & Chung, J. D. (2019). Unsteady squeezing carbon nanotubes based nano-liquid flow with Cattaneo–Christov heat flux and homogeneous–heterogeneous reactions. Applied Nanoscience, 9(2), 169-178.

[44] Chaudhary, M. A., & Merkin, J. H. (1995). A simple isothermal model for homogeneous-heterogeneous reactions in boundary-layer flow. I Equal diffusivities. Fluid Dynamics Research, 16(6), 311.

[45] Hayat, T., Muhammad, K., Farooq, M., & Alsaedi, A. (2016). Unsteady squeezing flow of carbon nanotubes with convective boundary conditions. PloS One, 11(5).

[46] Rosseland, S. (1931). Astrophysics and nuclear-theoretical foundations. 41-44.

Nomana thesis

ORIGINALITY REPORT

12%	3%	7%	7%
SIMILARITY INDEX	INTERNET SOURCES	PUBLICATIONS	STUDENT PAPERS

PRIMARY SOURCES

1	Submitted to Higher Education Commission Pakistan Student Paper	5%
2	Dianchen Lu, Zhixiong Li, M. Ramzan, Ahmad Shafee, Jae Dong Chung. "Unsteady squeezing carbon nanotubes based nano-liquid flow with Cattaneo–Christov heat flux and homogeneous–heterogeneous reactions", Applied Nanoscience, 2018 Publication	2%
3	link.springer.com Internet Source	1%
4	ANUM SHAFIQ, SUMAIRA JABEEN, T. HAYAT, A. ALSAEDI. "CATTANEO–CHRISTOV HEAT FLUX MODEL FOR SQUEEZED FLOW OF THIRD GRADE FLUID", Surface Review and Letters, 2017 Publication	<1%
5	Submitted to Universiti Putra Malaysia Student Paper	<1%